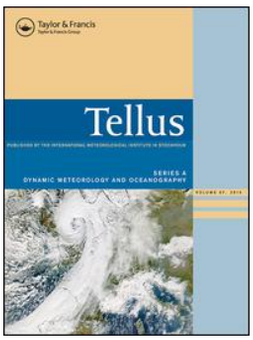

Tellus A: Dynamic Meteorology and Oceanography

ISSN: (Print) 1600-0870 (Online) Journal homepage: https://www.tandfonline.com/loi/zela20

On statistics of the free-troposphere synoptic component: an evaluation of skewnesses and mixed third-order moments contribution to the synoptic-scale dynamics and fluxes of heat and humidity

Vladimir Petoukhov, Alexey V. Eliseev, Rupert Klein & Hermann Oesterle

To cite this article: Vladimir Petoukhov, Alexey V. Eliseev, Rupert Klein & Hermann Oesterle (2008) On statistics of the free-troposphere synoptic component: an evaluation of skewnesses and mixed third-order moments contribution to the synoptic-scale dynamics and fluxes of heat and humidity, Tellus A: Dynamic Meteorology and Oceanography, 60:1, 11-31, DOI: 10.1111/j.1600-0870.2007.00276.x

To link to this article: https://doi.org/10.1111/j.1600-0870.2007.00276.x

Published online: 15 Dec 2016.

Tellus (2008), 60A, 11–31
Printed in Singapore. All rights reserved

TELLUS

On statistics of the free-troposphere synoptic component: an evaluation of skewnesses and mixed third-order moments contribution to the synoptic-scale dynamics and fluxes of heat and humidity

By VLADIMIR PETOUKHOV[1]*, ALEXEY V. ELISEEV[2], RUPERT KLEIN[1], and HERMANN OESTERLE[1], [1]*Potsdam Institute for Climate Impact Research, A26 Telegrafenberg, 14473 Potsdam, Germany;* [2]*A.M. Obukhov Institute of Atmospheric Physics RAS, 3 Pyzhevsky, 119017 Moscow, Russia*

(Manuscript received 17 October 2006; in final form 21 August 2007)

ABSTRACT

Based on the ERA40 data for 1976–2002 we calculated skewnesses and mixed third-order statistical moments (TOMs) for the synoptic variations [with (2.5–6) d timescales] of horizontal winds, temperature, vertical velocity and the specific humidity in Eulerian coordinates. All these variables show skewnesses which markedly deviate from zero, basically at the entries and the outlets of the mid-latitude storm tracks. In these regions, high values of skewness for vertical velocity, temperature and the specific humidity are revealed throughout the entire free troposphere, while the marked skewnesses for horizontal winds are traced in the lower free troposphere. We found a notable deviation of the synoptic-component statistics from the Gaussian statistics. We also made an estimate of the contribution from TOMs to the prognostic equations for the synoptic-scale kinetic energy and the meridional fluxes of sensible and latent heat, which appeared to be non-negligible, mainly in the storm tracks in winter. Our analysis attests that the most pronounced contribution of TOMs to the aforementioned equations comes from the self-advection by the horizontal synoptic-scale motions, while the TOMs induced by the metric terms in the original equations, and specifically the TOMs associated with the vertical self-advection by the synoptic-scale motions, are much less important.

1. Introduction

In many observational and model studies of the Earth's climate (see, e.g. Oort, 1983; Claussen et al., 2002), it is conventional to represent the synoptic-scale atmospheric components in terms of their statistical moments. This method is employed, in particular, in statistical-dynamical climate models and, more recently, Earth system models of intermediate complexity (EMICs) (Saltzman, 1978; Claussen et al., 2002; Petoukhov et al., 2005). In most of these models, the atmospheric climate statistics (e.g. monthly and long-term means and variances) appear as dependent variables governed by appropriate evolution equations. To derive, for example, the equations for such means (long-term 'climate' variables) the original primitive atmospheric equations of motion, the thermodynamic equation, and the water vapour balance equation are subjected to the corresponding time averaging. Mathematically, this method is analogous to the ensemble averaging in the theory of turbulence (see, e.g. Monin and Yaglom, 1981; McComb, 1992). Usually, the equations for the atmospheric means are equivalent to the Reynolds equations but with the cross- and autocovariances of the 'weather' terms (the second-order statistical moments for synoptics) substituted for the Reynolds stresses.

A common problem involved when employing this approach is the closure procedure for the second-order moments (SOMs). The simplest way to solve this problem is to use a diffusion approximation for SOMs (Defant, 1921; Williams and Davies, 1965; Green, 1970; Pavan and Held, 1996; Schmittner et al., 2000). This approximation is most appropriate for the description of the global-scale meridional synoptic fluxes (Srivatsangam, 1978; Lorenz, 1979).

Another way to close SOMs is to treat them in terms of the most linearly unstable baroclinic mode (Saltzman and Vernekar, 1971). Based on this assumption Stone (1978) formulated the concept of baroclinic adjustment and Branscome (1983) derived the corresponding parametrization for the meridional heat flux. However, as was shown in (Farrell, 1982, 1984), the most linearly unstable wave begins to dominate at timescales which are

*Corresponding author.
e-mail: petukhov@pik-potsdam.de
DOI: 10.1111/j.1600-0870.2007.00276.x

larger than the characteristic timescale of the synoptic eddy life cycle. Welch and Tung (1998a) demonstrated that the most unstable wave needs not be the dominant wave in the meridional heat fluxes, due to the non-linear processes of saturation and breakdown. By non-linear mechanisms, the energy of this mode can be transferred to smaller zonal wavenumbers (5–6, according to Randel and Held, 1991), which dominate the heat fluxes. On the other hand, Branstator (1995) satisfactorily approximated the synoptic eddy statistics as the statistics of random initial disturbances evolving linearly on the background flow over a prescribed time interval.

Following the ideas of early investigations into homogeneous turbulence (e.g. Kraichnan, 1959), Farrell and Ioannou (1994) proposed a parametrization for the meridional heat flux, based on a stochastic-process representation (with some dissipation accounted for) of the quadratic non-linearities in the governing equations, which allowed them to reduce those equations to a multilinear Markov process. With the use of a general circulation model (GCM), their parametrization has been tested by Zhang and Held (1999), who found that the latter was able to reproduce some important features of the meridional heat flux. Whitaker and Sardeshmukh (1998) modelled the statistics of the extratropical synoptic eddies assuming that those eddies were stochastically forced by Gaussian white noise and stabilized with damping operator on a baroclinically stable background flow. Yet in (Sura et al., 2005), a quasi-linear dynamical system stochastically perturbed by a multiplicative noise from unresolved components was proposed as a paradigm for non-Gaussian statistics demonstrated by some atmospheric circulation systems, such as damping quasi-linear Rossby waves.

In (Defant, 1921; Monin, 1958; Kurihara, 1970; Egger, 1975; Opsteegh and van den Dool, 1979; Petoukhov, 1980; Petoukhov et al., 1998; Handorf et al., 1999; Petoukhov et al., 2000), the corresponding equations for SOM dynamics were developed starting from the original primitive equations. This approach invokes a problem of the description and evaluation of the contribution from the triple correlations of the synoptic-scale disturbances to the equations for SOMs. As an example, the equation for the synoptic-scale kinetic energy E_s has been studied in Kurihara (1970) and Lau (1979). Kurihara (1970) employed, in particular, a zonally averaged equation for E_s in his statistical-dynamical atmospheric model. Lau (1979) investigated contribution from several terms to a non-zonal equation for E_s at 300 hPa ignoring, however, those terms which include the vertical motions. In this latter paper, it was shown that the contribution from the third-order moments (TOMs) to the equation for E_s is non-negligible. This statement is also supported by the results of Saltzman et al. (1961), based on the hemispheric 500 hPa data for the particular year of 1951, and by Opsteegh and van den Dool (1979) for the winter of 1976/1977 at different vertical levels over the northwestern Europe.

A significant skewness for the observed synoptic fluctuations of geopotential height Φ has been noted by Holzer (1996). In that paper, temporally raw and spatially filtered—by eliminating the planetary wavenumbers less than 8—fields of Φ were analysed for the period December 1978 to August 1988. With the use of a 15-yr (1972–1986) observational time series, Swanson and Pierrehumbert (1997) investigated the probability density functions (PDFs) for the synoptic disturbances of temperature and meridional velocity in the lower troposphere of the Pacific storm track and demonstrated notable skewnesses for both the variables. This may imply non-negligible values of the third-order moments built on the indicated quantities.

There exists, however, some controversy in the literature regarding the importance of the role TOMs play on the synoptic timescale. In contrast to the above-mentioned papers, White (1980) has exhibited only statistically insignificant skewness for the geopotential height, which values were estimated using 2.5–6 d bandpass filtered time series for the 11 winters from 1965–1966 to 1975–1976 over the Northern Hemisphere. Weaver and Ramanathan (1997) reported on close-to-Gaussian distributions for the vertical velocity fluctuations at 500 hPa over the entire North Pacific and North Atlantic storm tracks for January and July of 1985–1989.

In this connection it should be noted that most of the statistical-dynamical climate models, conceptual stochastic climate models and EMICs (see, e.g. Green, 1970; Egger, 1975; Branscome, 1983; Farrell and Ioannou, 1994; Handorf et al., 1999) apply diffusion (gradient) approximations for the synoptic-scale fluxes of momentum, heat and moisture, which can be justified under the assumption of Gaussian statistics for the sets of the corresponding meteorological variables. The validity of the mentioned approximations is not evident, and a problem of the advection-diffusion nature of the synoptic-scale transports of different quantities arises (Pierrehumbert, 1991; Hu and Pierrehumbert, 2001). Also, the individual synoptic eddies/waves possess a quasi-conservative internal structure (Simmons and Hoskins, 1978, 1980; Sinclair, 1997; Methven and Hoskins, 1998), which interacts with its environment (Lorenz and Hartmann, 2001; Fantini, 2004), and their characteristic spatial scale and 'mixing length' (displacement) can be comparable to the spatial scale of the basic flow (Green, 1970; Rhines, 1975; Larichev and Held, 1995). In some cases, Gaussianity may violate the realisability conditions, as was demonstrated for small-scale turbulence and convection in the planetary boundary layer (Ogura, 1962; Schumann, 1977; Salmon, 1998; Gryanik and Hartmann, 2002; Gryanik et al., 2005). All these circumstances make it problematic an application of the Gaussian model to the description of the synoptic component of the atmosphere.

Another example regarding a possible importance of TOMs concerns the role of the non-linear wave–wave interaction at the growth stage of the baroclinic eddies. Since TOMs (as well as skewness) can be a signature of this underlying non-linearity (Holzer, 1996; Rivin and Tziperman, 1997), ignoring the triple correlations of synoptic eddy quantities is equivalent to neglecting leading order of the wave–wave interactions. As is shown

by Farrell (1982, 1984), the latter can play an important role in the dynamics of the growing baroclinic waves. In this respect, neglect of TOMs in the parametrized synoptic-scale dynamics can distort the underlying physics of the baroclinic disturbances and their interaction with a background flow.

The goal of this paper is to complement the above-mentioned investigations into the role of TOMs in the synoptic-scale dynamics and thermodynamics through the analyses of more extensive data and to reveal, for which variables and in which regions of the free troposphere the assumption on the synoptic eddy Gaussian statistics is or is not valid. For that purpose, we employ the state-of-the-art 27-yr (1976–2002) daily sampled time series of ERA40 reanalysis data, with global coverage at five tropospheric pressure levels. The method of data processing we use to derive the statistical characteristics of the synoptic-scale atmospheric component is described in Section 2. Section 3.1 presents the results of calculations of skewnesses for a set of the basic synoptic-scale variables. The obtained in Section 3.1 results reveal a notable deviation of the synoptic-component statistics from Gaussian statistics, mostly in the mid-latitude storm tracks, over the subtropical regions with high anticyclonic activity, and in the locations of the intense cyclogenesis over the Polar Southern Ocean. Also, in Section 3.1 we discuss some feasible phenomenological and physical factors that can cause deviations of the synoptic-scale statistics from Gaussian statistics, in terms of skewness. Besides, Section 3.1 addresses possible reasons for the discrepancy between the results presented in the cited above papers, with respect to the statistical significance of skewness of the synoptic-scale atmospheric fields. In Section 3.2, the contributions from different TOMs to the equation for the synoptic-scale kinetic energy are estimated, which appear to be non-negligible, mainly in the storm tracks in winter. In Section 3.3, we analyse the role the third-order moments play in the equations for the synoptic-scale meridional fluxes of heat and moisture. It is found that these latter moments attain one-tenth to one-third the corresponding second-order moments in the above-mentioned equations, in the storm tracks in winter, and hence cannot be neglected in those equations. In Section 4, an overall discussion of the presented results is given and a hypothesis is outlined for the profound linkage between the intrinsic non-linear structure and spatial inhomogeneity of the synoptic systems, on the one hand, and skewnesses of the synoptic-scale components of the free troposphere, on the other.

2. The method of data processing

We use as the initial data the daily arrays of zonal and meridional winds (u and v, respectively), vertical velocity in pressure coordinates ω, temperature T, and the specific humidity q from the ERA40 reanalysis data set (Simmons and Gibson, 2000) for 1976–2002 at five atmopsheric levels (850, 700, 500 400 and 300 hPa). The horizontal resolution of the data is $2.5^\circ \times 2.5^\circ$ latitude and longitude. We note that the key results of this paper for the Northern Hemisphere (NH) have also been reproduced when using the 6-hourly ERA40 reanalysis data for the NH, as well as when employing different subsamples of the total set of the ERA40 reanalysis data for 1976–2002. We did not exploit in our analysis the total 45-yr archive of the ERA40 reanalysis data because of a rather low reliability of the data obtained prior to 1976, and due to possible artefacts caused by changes in the observing system in the early/middle seventies (Bengtsson et al., 2004a,b).

The synoptic-scale variations X' ($X = u, v, \omega, T, q$) have been extracted from the above-mentioned raw data applying the recursive bandpass filter developed by Murakami (1979). The same filter has been previously used by Christoph et al. (1995) to study the intraseasonal storm track variability. In this latter paper, it was shown that the indicated filter extracts the synoptic scales with an accuracy close to that achieved when employing a more sophisticated filter originally proposed in (Blackmon, 1976) and exploited later on by Lau and Wallace (1979), Lau (1979, 1988), White (1980) and Lau and Wallace (1979). Compared to the Blackmon filter, the Murakami filter cuts a smaller number of points in the time series for the atmospheric variables and allows one to construct longer time series with weaker restrictions on the statistical significance of the obtained results. Following conventional procedures (Blackmon, 1976; Lau, 1979; Lau and Wallace, 1979; White, 1980; Lau, 1988; Christoph et al., 1995) we have chosen the lower and the upper cut-off timescales at 2.5 and 6 d, respectively [while Trenberth (1991) and Nakamura and Shimpo (2004) have used a somewhat wider (2.5–8) d band]. Let us note that we repeated our calculations with the use of a variety of the bandpass filter lower and upper cut-off timescales, correspondingly, in the 2.1–2.5 and 6.0–8 d ranges, to be certain in the stability of the results of our calculations of skewnesses and TOMs. In this, all the results discussed in the following have been well reproduced.

In the present paper, the aforementioned bandpass filtering has been applied to the initial reanalysis data for each month, from January 1976 to December 2002. Then the bandpass filtered data, for a given calendar month of all the years from 1976 to 2002, have been combined and the resulting time series has been used to compute the sampled statistical moments for this month. Alternatively, the sampled statistical moments have been first computed for a given calendar month of each year independently, and then they were averaged over all the years. Both approaches give close results but with a lower statistical significance for the latter. Below, only the results for the first approach are presented.

As discussed in Section 1, a convenient measure for deviations from a normal distribution, which gives clues to the importance of the synoptic-scale third-order moments, is the non-standardized skewness of the synoptic fluctuations (see Abramowitz and Stegun, 1972)

$$S = \frac{\overline{X'^3}}{\overline{X'^2}^{3/2}},$$

A statistical significance of departure, in terms of skewness, of a given sampled stochastic process from a Gaussian process can be assessed using the sampled standard deviations $\sigma_{S,G}$ for the Gaussian skewness, where (see, e.g. Abramowitz and Stegun, 1972; Holzer, 1996)

$$\sigma_{S,G} = (6/N_{\text{eff}})^{1/2}.$$

Here N_{eff} designates the number of degrees of freedom in the bandpass-filtered time series. The number of degrees of freedom has been estimated as $N_{\text{eff}} = N\,(1 - r_1)/(1 + r_1)$ (Holzer, 1996), where r_1 is lag-1 autocorrelation in the time series for given geographic location and calendar month. In this, a stochastic process is assumed to be non-Gaussian if the standardized (divided by $\sigma_{S,G}$) skewness, S_{st}, is larger in magnitude than 2 (Holzer, 1996). As shown in (Holzer, 1996), this method for the estimation of the statistical significance of the deviation from Gaussianity yields results, which closely match those obtained with the use of more elaborated methods, and thus S_{st} can serve as a reliable criterion for the assessment of non-Gaussianity of a sampled stochastic process. However, division by $\sigma_{S,G}$, which depends itself on the geographic location and calendar month, may distort spatial and temporal structure of the non-standardized skewness S and obscure the interpretation of the physical background for the latter. Also, the usage of S_{st} prevents a direct comparison between skewnesses of different stochastic fields. For the above-mentioned reasons, both the non-standardized and standardized skewnesses are presented in our paper for all the atmospheric variables under discussion.

3. Results

3.1. Skewnesses of synoptic-scale variations

Among the synoptic-scale atmospheric variables studied in this paper, vertical velocity, temperature, and the specific humidity exhibit the most marked skewness, mainly in the areas of high cyclonic activity in the mid-latitude storm tracks. A statistically significant skewness is found for these variables at all the considered tropospheric levels in the indicated areas.

3.1.1. Vertical velocity. Figure 1a–f presents the non-standardized synoptic-scale ω- velocity skewness, $S_{\omega'}$, for the lower (Fig. 1a and b), middle (Fig. 1c and d), and upper (Fig. 1e and f) free troposphere.

As seen in Fig. 1a and b, ω-velocity is skewed negatively on the synoptic scale in the lower free troposphere over most of the oceanic regions for all seasons in both Hemispheres. [Let us recall that the negative values of ω correspond to the ascending atmospheric motions.] The geographic regions occupied by the main mid-latitude storm tracks (see, e.g. Petterssen, 1950; Wallace et al., 1988; Sinclair and Watterson, 1999; Simmonds and Keay, 2000; James, 2001; Trigo, 2006) are clearly delineated in Fig. 1a and b by relatively high [up to $-(0.6$–$0.8)$] negative values of $S_{\omega'}$. These regions are more spacious in winter for both Hemispheres, which is in line with the observed larger areas of the winter mid-latitude storm tracks relative to their summer counterparts (James, 2001). Also, as seen in Fig. 1a and b all the mid-latitude storm tracks exhibit by and large higher (in magnitude) values of $S_{\omega'}$ in the lower troposphere in winter.

Presumably, the above-mentioned phenomenological features of the geographic and seasonal distribution of $S_{\omega'}$ in the lower troposphere of the storm tracks can result from the specific features of the ensembles of the mid-latitude travelling cyclonic systems. These systems are strongly non-linear finite-amplitude baroclinic structures (eddies/waves) and possess high spatial inhomogeneity, that is, they usually consist of two distinctly different spatial substructures: (a) rather concentrated non-linear cyclonic vortex, with relatively strong and overall upward vertical motions and (b) more spacious baroclinic zone accompanying the vortex, with more sluggish and by and large downward vertical motions. The mentioned baroclinic zones include, in the general case, the extended areas with moderate horizontal gradients of the atmospheric fields and the narrow regions of atmospheric fronts, which can connect the cyclonic vortices (Balasubramanian and Yau, 1996; Methven and Hoskins, 1998; Welch and Tung, 1998a,b; Hakim et al., 2002). Let us notice that the bandpass filtering and spatial resolution chosen in our paper allow us to trace, without a marked distortion, both the substructures (a) and (b) of the cyclonic systems in the mid-latitude storm tracks.

As shown in (Lapeyre and Held, 2004), the latent heating distinctly affects the characteristic value of the vorticity skewness $S_{\zeta'}$ for the ensembles of the cyclonic systems in the mid-latitude lower troposphere. In doing so, the stronger is the latent heating the higher is the positive values of $S_{\zeta'}$ (Lapeyre and Held, 2004). Furthermore, $S_{\zeta'}$ in the lower troposphere is positively correlated with $S_{w'}$ (Wiin-Nielsen, 1974) (where w is the vertical velocity in the Cartesian coordinates), in particular, in the mentioned cyclonic ensembles. In this, both ζ' and w' are basically localized within the indicated substructures (a) (concentrated vortices) of the cyclonic systems. As far as the latent heat release due to the condensation is higher in the lower troposphere of the storm tracks of both Hemispheres in winter, as compared to summer (see, e.g. fig. 7.24 in Peixoto and Oort, 1992), this can be according to (Lapeyre and Held, 2004) a reason for higher positive values of $S_{\zeta'}$ in winter, and may cause in line with (Wiin-Nielsen, 1974) higher positive (negative) values of $S_{w'}(S_{\omega'})$ in this season within the considered part of the atmosphere. We note that a pronounced anticorrelation between $S_{\zeta'}$ (and hence $S_{w'}$) and the ensemble-mean fractional area A_p of the precipitation in the lower troposphere is neatly traced in (Lapeyre and Held, 2004) by the comparison of figs. 5b and 12b from the cited paper. Since A_p in (Lapeyre and Held, 2004) is substantially determined by the fractional area $A_{+,w'}$ occupied by the concentrated cyclonic vortices with an overall upward motions within them, this gives a rather straightforward indication of a strong anticorrelation between $A_{+,w'}$ and $S_{w'}$. In this, a (positive) sign of $S_{w'}$ over the total

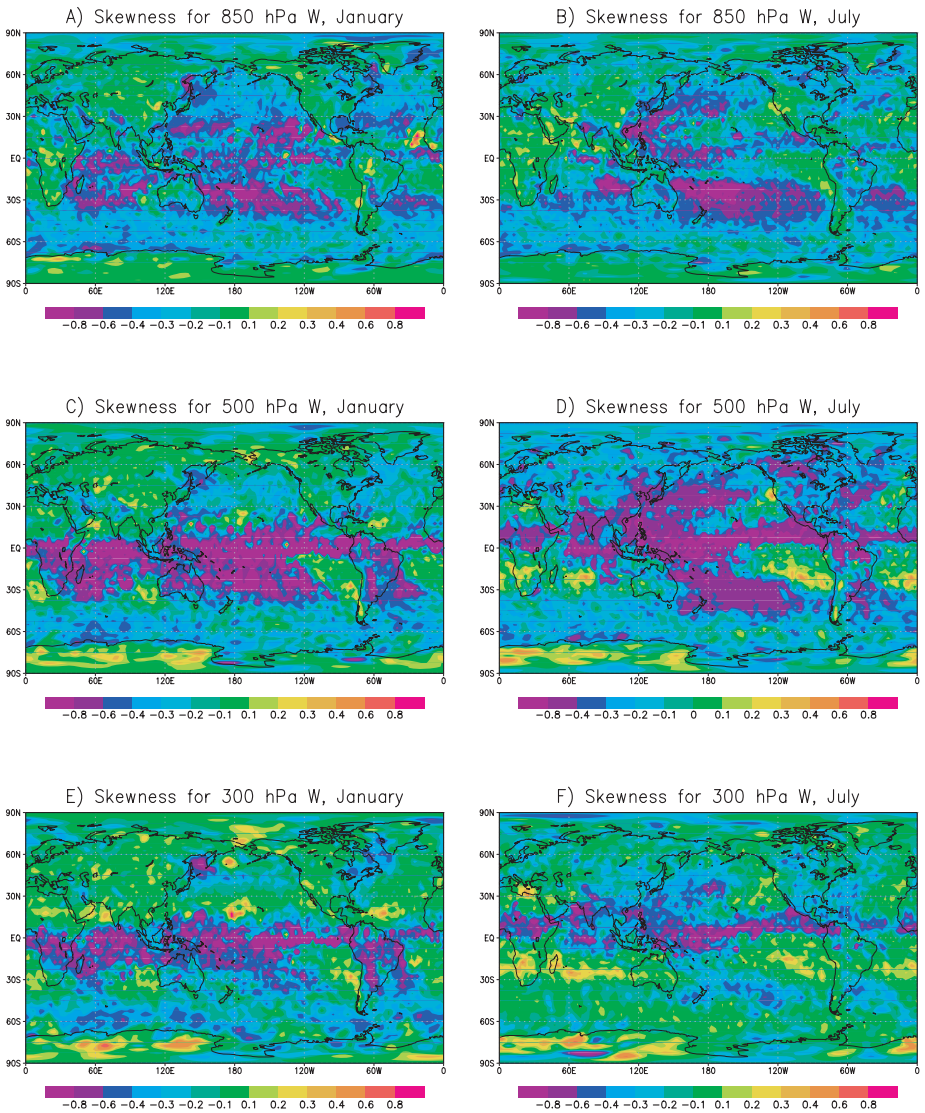

Fig. 1. Skewness for the synoptic-scale ω-velocity fluctuations at 850 hPa (a, b), 500 hPa (c, d) and 300 hPa (e, f) for January (a, c, e) and July (b, d, f).

area coincides with a dominant sign of w' within the concentrated cyclonic vortices.

Our results suggest that the mid-latitude oceanic storm tracks are well followed also in the middle troposphere of both Hemispheres, in terms of the marked negative values of $S_{\omega'}$ (see Fig. 1c and d). Furthermore, unlike the lower free troposphere, the middle troposphere by and large exibits more spacious areas with high negative values of $S_{\omega'}$ in the oceanic mid-latitude storm tracks in summer (cf. Fig. 1c and d). With an eye to what was discussed in the previous paragraph, this can be a consequence, in particular, of a minor role the hydrological processes play within the considered range of heights in the middle latitudes in winter, as compared to summer. The latter circumstance is demonstrated, for example, by fig. 12.5 in (Peixoto and Oort, 1992) and figs. 16 and 17 in (Lorenz, 1967).

As is seen from Fig. 1a–d, $S_{\omega'}$ decreases in magnitude from the locations of the cyclone eddy generation, at the mid-latitude storm track entries, to those of the eddy dissipation, at the storm track outlets, for winter and summer in the lower and the middle free troposphere of both Hemispheres. Most likely this peculiarity can be explained accounting for the upstream-to-downstream evolution of the characteristic features of the cyclonic systems within the mid-latitude storm tracks. The indicated evolution manifests itself in the gradual increase in the size of the concentrated cyclonic eddies [the above-mentioned spatial substructure (a)], which the latter experience in the course of their life cycle, from the generation to the occlusion and dissipation, via the maturity stage. This latter process is accompanied by the barotropization and the decrease in the characteristic value of w' within the eddies, specifically over the land masses with

relatively low (high), as compared to the oceanic regions, latent heat forcing (roughness) (Simmonds, 2000).

The specific feature of the more extended regions with high negative values for $S_{\omega'}$ in summer (as in the middle troposphere) and a decrease in the magnitude of $S_{\omega'}$ from the locations of the cyclone eddy generation to those of the eddy dissipation (as in the lower and the middle troposphere) are well traced also in the upper troposphere of the mid-latitude storm tracks (Fig. 1e and f). The reason for that can be the same as for the discussed above similar peculiarities of the synoptic-scale ensembles in the lower and middle troposphere. In this, $S_{\omega'}$ is much less distinct in the upper troposphere as a whole in the mid-latitude storm tracks in comparison with the lower and middle troposphere in those regions (cf. Fig. 1–f). This can be associated with an overall change in the physical properties and horizontal spatial structure of the cyclonic systems from the lower to the upper troposphere. Namely, the mentioned systems become in the upper troposphere much more dry and more close to the linear wave-like structures (James, 1952; Wallace et al., 1988; Chang, 1993; Chang and Orlanski, 1993; Orlanski and Gross, 2000). As can be inferred from the preceding, both the indicated factors favour a decrease in the magnitude of $S_{\omega'}$, in particular, due to a decrease in the non-linearity and spatial inhomogeneity of the cyclonic systems.

Well-marked regions with high negative values of $S_{\omega'}$ over the Polar Southern Ocean in the vicinity of the Antarctic margin are yet another important feature of the synoptic-scale component of the vertical velocity in the lower free troposphere, which is demonstrated by Fig. 1a and b. These regions are just the locations of the intense cyclogenesis over the Polar Southern Ocean (see, e.g. Bromwich, 1991; Fitch and Carleton, 1991). Also, the areas of the intense generation of the cyclonic vortices over the Weddell Sea and the Ross Sea (e.g. Heinemann, 1990; Heinemann and Klein, 2003) have marked fingerprints in Fig. 1a and b: these are seen as the locations of high negative values of $S_{\omega'}$. As illustrated in Fig. 1c–f, the above-mentioned regions of the intense cyclogenesis over the Polar Southern Ocean and in the Weddell Sea and the Ross Sea are observed also in the middle and upper troposphere, specifically in the austral summer. As may be inferred from Fig. 1a–f, the phenomenological structure of $S_{\omega'}$ over the Polar Southern Ocean is close to the discussed above for the mid-latitude storm tracks. We call attention to the coincidence of a sign for S'_w in the locations of the cyclogenesis over the Polar Southern Ocean as a whole with a dominated sign of w' developed within the concentrated cyclonic vortices in the ensembles of the synoptic systems there.

Let us notice that we cannot, of course, rule out the alternative explanations for non-Gaussian behaviour of the ensembles of the cyclone systems in the mid-latitude storm tracks. For instance, the storm track dynamics can be inherently Gaussian, but over longer timescale than the upper cut-off timescale used in our paper the storm tracks change position, for example, moving further poleward or equatorward with the jetstreams. The Eulerian statistics presented in the paper may then sample from different normal distributions resulting in a marked skewness. In the end of Section 3.1, we discuss some other phenomenological features of the large-scale atmospheric dynamics, as well as the physical mechanisms, which can result in non-Gaussian statistics for the synoptic component in the free troposphere.

Rather distinctly traced in Fig. 1a–f are the areas with high positive (negative) values of $S_{\omega'}(S'_w)$ in the principle axes of the mid-latitude anticyclone propagation. For instance, as is demonstrated by Fig. 1a, c and e the locations of high anticyclonic activity are followed for the NH winter by the marked positive values of $S_{\omega'}$ to the east of the Caspian Sea, over the Mongolia, in the polar and mid-latitude North America along (and at some distance from) its western coast, over the northeastern part of the North Africa, and in the axes of propagation of the subtropical anticyclones over the North Pacific and North Atlantic, with the extension of the paths of the Atlanic anticyclones to Europe (Petterssen, 1950; Palmen and Newton, 1969). Unlike the cyclonic areas, the principal trajectories of the mid-latitude and subtropical anticyclones are by and large more clearly traced in Fig. 1a–f in the middle and the upper troposphere. Apparently, this is due to a pronounced barotropic component in the vertical structure of the anticyclones (Chen et al., 2001), as compared to their cyclonic (especially tropical cyclonic Hsu, 2005) counterparts. As in the case with the storm-track cyclonic systems, the geographic and seasonal distribution of $S_{\omega'}$ in the regions of high anticyclonic activity illustrated by Fig. 1a–f can result from the specific features of the ensembles of the travelling anticyclonic systems as the totality of the concentrated nonlinear finite-amplitude quasi-barotropic vortices embedded into the more spacious accompanying baroclinic zones. The indicated anticyclonic systems are characterized by rather strong descending as a whole vertical motions with negative values of w' in the concentrated anticyclonic vortices and much more sluggish and by and large ascending vertical motions in the accompanying baroclinic zones. Again, a sign of $S_w{}'$ over the areas of high anticyclonic activity, as a whole, coincides with a dominant sign of w' within the spatial substructures (a) (concentrated anticyclonic eddies) in the ensembles of the anticyclonic systems.

The locations of the quasi-permanent anticyclones are also clearly seen in Fig. 1a–f, although at first sight their temporal scales are far beyond the range of the periods embraced by the upper and lower cut-off timescales we use in this paper. Nonetheless, the Siberian High manifests itself in Fig. 1a, c and e as the region with rather notable positive values of $S_{\omega'}$ in the 100–120 E, 40–60 N longitudinal/latitudinal range at all the studied atmospheric levels in winter. Also, the pronounced positive values of $S_{\omega'}$ in Fig. 1a–f mark the position of the Azores High, with the intrinsic seasonal and vertical structure of that quasi-stationary system being well followed. The analogous structure of the $S_{\omega'}$ field is traced in the location of the North Pacific (Californian) High. This latter pattern is more distinct in summer (cf. Fig. 1a, c, e and Fig. 1b, d, f, respectively), which fits well the seasonal cycle for the magnitude of the indicated High.

The above-mentioned quasi-permanent anticyclones are featured by an overall subsidence of the air within them (Corte-Real et al., 1998; Cohen et al., 2001; Bograd et al., 2002). In doing so, these systems can be distinctly 'exposed' in the field of the synoptic-scale vertical velocity skewness, due to, for example, a 'pulse' phenomenon, which is exhibited by these objects on the synoptic time scale (see Palmen and Newton, 1969; Lamb, 1975; Davis et al., 1996). As is shown in (Lamb, 1975), the indicated phenomenon results in the pronounced change in the position and intensity of the quasi-permanent anticyclones between consecutive, approximately 5–6 d, periods assosiated essentially with the passage of (and the corresponding interaction with) the flowing anticyclones.

Figure 1b, d and f demonstrates also a close linkage between the monsoons and the synoptic-scale cyclonic activity which is claimed in a large number of the publications on the issue (see Ramage, 1971; Knox, 1987; Mak, 1987; Palmer, 1994; Hoskins, 1996; Tomas and Webster, 1997; Webster et al., 1998; Rodwell and Hoskins, 2001; Goswami et al., 2003). In particular, the specific feature of the Indian summer monsoon is traced by the corresponding pattern of high negative values of $S_{\omega'}$ in the Ganges valley, which marks the passage of the numerous continental cyclones over the region (Fig. 1b). The South American summer monsoon manifests itself in Fig. 1a, c and e by the analogous to the Indian monsoon high negative values of $S_{\omega'}$ over the land masses, which capture the geographic locations of strong ascending motions on the synoptic timescales in that area (Jones and Carvalho, 2002).

Figure 1a–f shows high negative values for $S_{\omega'}$ in the tropics, especially in the location of the ascending branch of the Hadley circulation, the Intertropical Convergence Zone (ITCZ). This can be brought about by the intrusions to the tropics of the synoptic systems from the extratropical latitudes (see, e.g. Kiladis and Weickmann, 1992) and/or by the interaction of the ITCZ with the numerous synoptic-scale tropical eddies and waves (Riehl, 1979). Both these factors may, in particular, cause the local synoptic-scale displacements of the ITCZ axis position. Supposedly just the indicated forced displacements of the ITCZ axis can 'expose' the mentioned structure in the bandpass filtered and spatially resolved 'data' we use in our calculations.

The presented results testify that the vertical velocity skewness can be not only a signature of the underlying non-linearity of the synoptic processes but also it may serve as an indicator for the important large-scale quasi-stationary patterns of the atmospheric circulation, and the cyclone/anticyclone asymmetry inherent in the synoptic component of the atmospheric motions.

Figure 2a–f illustrates the geographic distribution of the standardized skewness of the synoptic-scale vertical velocity $S_{st,\omega'}$ at different atmospheric levels for January and July. The comparison of Figs. 1a–f and 2a–f attests that there exists a statistically significant departure, in terms of skewness, of a sampled stochastic process of the synoptic-scale vertical velocity from a Gaussian process in all the discussed above regions with high values of $S_{\omega'}$, as the absolute values of $S_{st,\omega'}$ in those regions are larger in magnitude than 2.

3.1.2. Temperature. The synoptic-scale temperature fluctuations in the NH exhibit statistically significant non-standardized skewness $S_{T'}$ at 850 hPa for January over the mid-latitude storm track areas in the upstream regions of the synoptic eddy generation, where $S_{T'}$ is positive (Fig. 3a). The analogous regions of the mid-latitude storm tracks in the SH with positive values of $S_{T'}$ are sharply defined at 850 hPa for July (see Fig. 3b). In both cases, the typical values of $S_{T'}$ are about +(0.3–0.6). In the summer Hemispheres, the above-mentioned peculiarity is less distinct over the indicated regions at this pressure level.

The subtropics in both Hemispheres, with the predominantly anticyclonic circulations, show negative values of the synoptic-scale temperature skewness at 850 hPa (Fig. 3a and b). The North Pacific (Californian) and Azores Highs are clearly followed, respectively, in the NH winter (Fig. 3a) and summer (Fig. 3b) by a relevant negative sign of $S_{T'}$ in those regions. The mid-latitude areas of the synoptic eddy dissipation in the outlet parts of the storm tracks are also featured with negative values of $S_{T'}$. This is seen in Fig. 3e and f, where the non-standardized skewness $S_{T'}$ for the synoptic-scale temperature fluctuations at 850 hPa is depicted, respectively, for the North Atlantic in January and for the South Pacific in July.

All the aforementioned in this subsection peculiarities of the $S_{T'}$ geographic distributions at 850 hPa are in line with the distributions for $S_{\omega'}$ described in the foregoing Section 3.1.1. In particular, negative values of $S_{T'}$ in the regions of the cyclone eddy occlusion and subsequent filling correspond to an overall cooling of the air in the lower layers within the cyclonic vortices in the process of cyclolysis (Morris and Smith, 2001). The latter results in a relatively more cold air in the uplifts within the concentrated cyclonic vortices at the considered final stage of the cyclone life cycle. As discussed previously, just these uplifts determine a negative sign of $S_{\omega'}$ in the outlets of the mid-latitude storm tracks. Such situation is opposite to the observed at the stage of young winter cyclones: these contain more warm air, as compared to the environment, due to the process of the cyclogenesis caused by, for example, the baroclinic instability or the explosive cyclogenesis. In this, overall updrafts within the concentrated cyclonic eddies bring about negative values of $S_{\omega'}$ in the corresponding upstream regions of the mid-latitude storm tracks, see Section 3.1.1 above. More warm (in comparison with the environment) air within young winter cyclones can result, in particular, from the intense latent heat release, specifically in the lower troposphere (Gyakim and Barker, 1988; Lapeyre and Held, 2004).

The locations of the intense cyclogenesis and convection over the Polar Southern Ocean also have a clear-cut fingerprint in Fig. 3a and b as regions with marked positive values of $S_{T'}$ for both January and July, with more high values in the austral summer. This fits well the discussed above distribution of $S_{\omega'}$ over the area (cf. Figs. 1a, b and 3a, b).

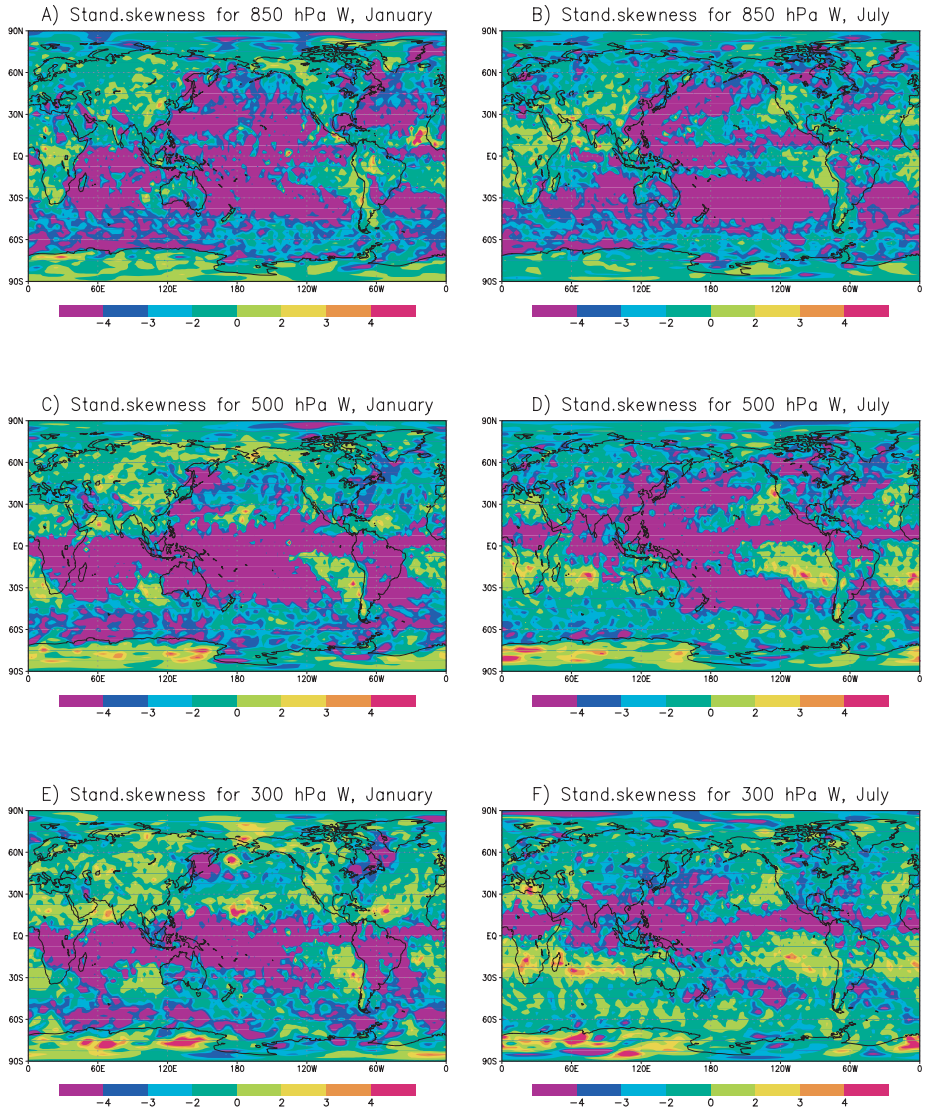

Fig. 2. Standardized skewness for the synoptic-scale ω-velocity fluctuations at 850 hPa (a, b), 500 hPa (c, d) and 300 hPa (e, f) for January (a, c, e) and July (b, d, f).

In the middle free troposphere (e.g. at 400 hPa, see Fig. 3c and d), the January pattern of the positive temperature skewness in the North Pacific storm track is more patchy than in the lower troposphere, while the North Atlantic storm track still exhibits a compact pattern of positive $S_{T'}$ amounting about +(0.3–0.6) (cf. Fig. 3a and c) for this month. In this, both the North Pacific and North Atlantic patterns of positive $S_{T'}$ are displaced to the west of their lower troposphere counterparts. This feature is in line with the results obtained in (Hoskins and Hodges, 2002) regarding the positions of the maxima for the 2–6-d bandpass filtered variances of temperature in the lower and upper troposphere (cf. figs. 3 and 4 in the cited paper). In the SH, a distinct signature of the South Pacific mid-latitude storm track is seen at 400 hPa for July, although this pattern of positive $S_{T'}$ is more weak and less aggregated than that in the lower troposphere (cf. Fig. 3b and d). The subtropical regions are characterized by a negative anticyclonic-type $S_{T'}$ at 400 hPa for both January and July in the NH and the SH (Fig. 3c and d). As in the lower troposphere (see Fig. 3a and b), the North Pacific High manifests itself in the middle troposphere in the same seasons (see Fig. 3c and d) as the location of high negative values of $S_{T'}$.

Figure 4a–d illustrates the geographic distribution of the standardized skewness of the synoptic-scale temperature perturbations $S_{st,T'}$ in the lower and middle free troposphere for January and July. The comparison of Figs. 3a–d and 4a–d testifies that the deviations, in terms of skewness, of a sampled stochastic process of the synoptic-scale temperature fluctuations from Gaussian process are statistically significant in all the discussed above regions with high values of $S_{T'}$, as far as the absolute values of $S_{st,T'}$ in those regions are larger in magnitude than 2.

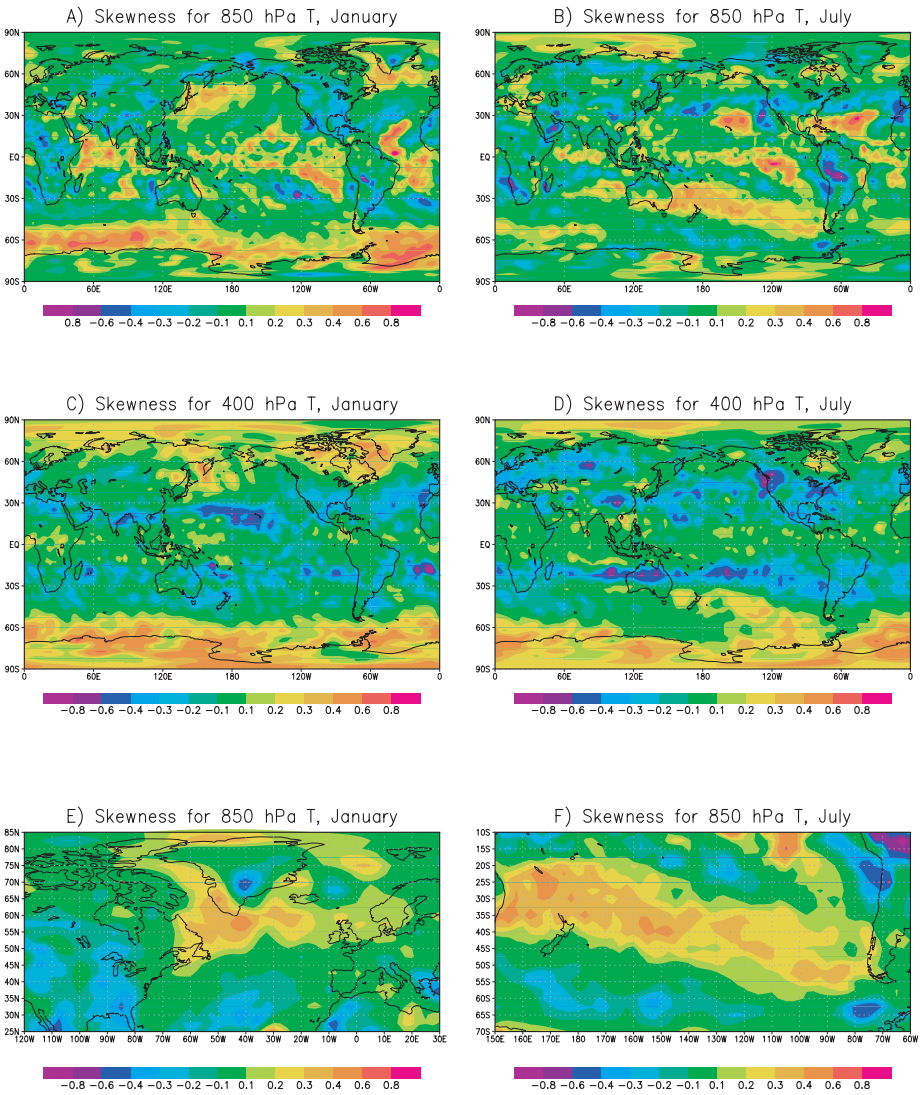

Fig. 3. Skewness for the synoptic-scale temperature fluctuations at 850 hPa (a, b) and 400 hPa (c, d) and the respective zoomed plots for 850 hPa in the North Atlantic (e) and the South Pacific (f) for January (a, c, e) and July (b, d, f).

3.1.3. Specific humidity. A distinct property of the geographic distribution for the lower- and mid-troposphere non-standardized skewness of the synoptic-scale specific humidity, $S_{q'}$, is the predominantly positive (negative) values of $S_{q'}$ in the polar regions (in the tropics) of both Hemispheres for January and July (Fig. 5).

The discussed in the foregoing sporadic invasions of the synoptic-scale systems from higher latitudes, with more dry, in the general case, air may be a reason for the observed in Fig. 5a and b geographic distribution of $S_{q'}$ in the tropics. On the other hand, the intrusions to the polar regions of the synoptic-scale systems with rather high moisture content in the concentrated vortices originating in the extratropical, subtropical, and even tropical latitudes, can bring about the phenomenological picture of $S_{q'}$ in the polar lower free troposphere (Fig. 5a and b). The synoptic-scale specific humidity is skewed positively at all the studied tropospheric levels in the mid-latitude oceanic storm track locations for both January and July (see Fig. 5). This feature suggests that the basic contribution to $S_{q'}$ in those regions can be assigned to positive values of q' in the concentrated cyclonic vortices with rather strong ascending vertical motions within them (Sinclair, 1997; Methven and Hoskins, 1998; Eckhardt et al., 2004), on the background of the predominantly northward (in the NH) and southward (in the SH) meridional component of the eddies' transport velocity in the presence of the overall pole-to-equator increase in the atmospheric specific humidity. In all the above-mentioned regions, $S_{q'}$ typically amounts +(0.6–0.8) or even higher values. Note that $S_{q'}$ is opposite in sign to $S_{T'}$ in the tropical lower troposphere (cf. Figs. 3a, b and 5a, b).

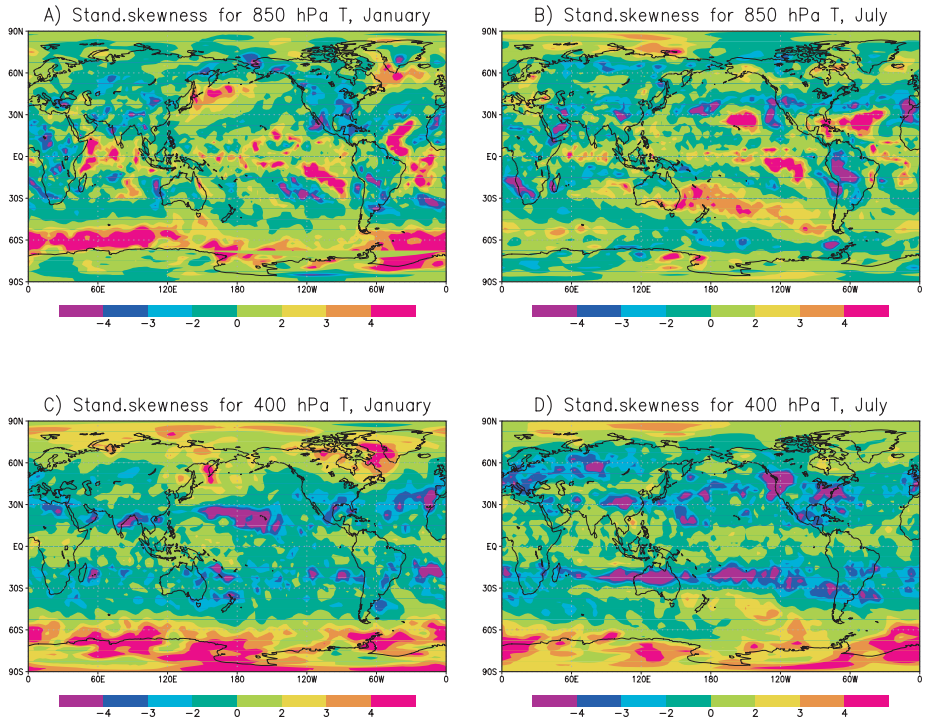

Fig. 4. Standardized skewness for the synoptic-scale temperature fluctuations for January (a, c) and July (b, d) at 850 hPa (a, b) and 400 hPa (c, d).

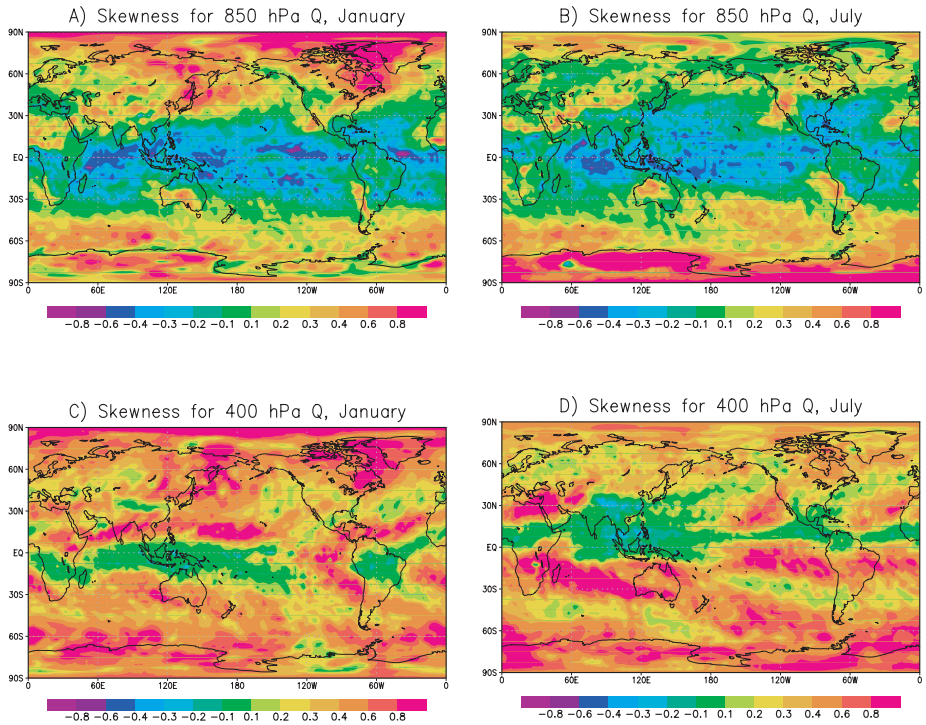

Fig. 5. Skewness for the fluctuations of the synoptic-scale specific humidity at 850 hPa (a, b) and 400 hPa (c, d) for January (a, c) and July (b, d).

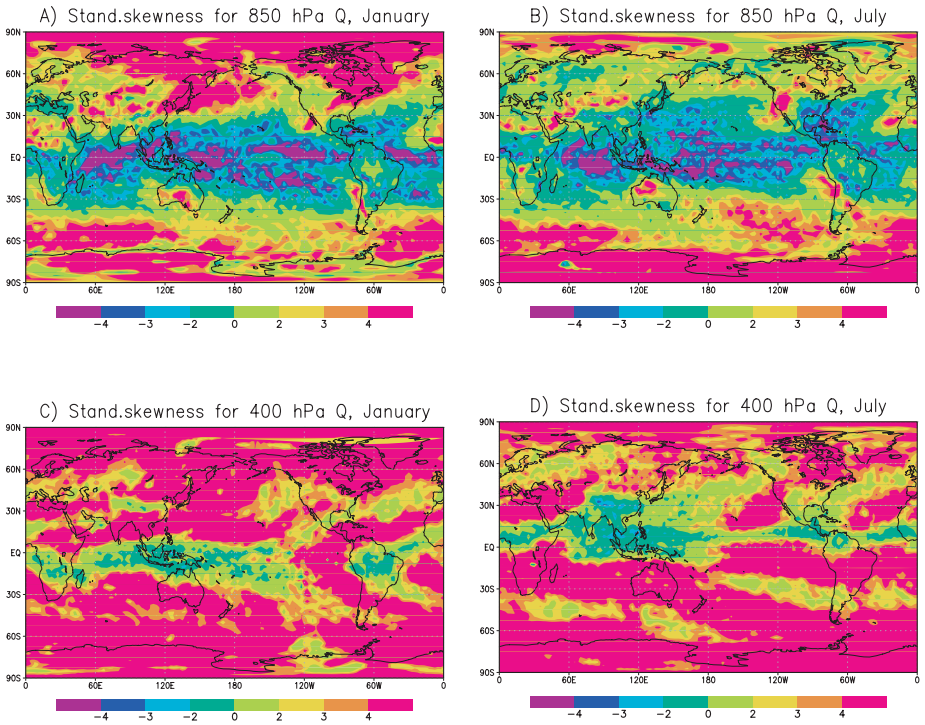

Fig. 6. Standardized skewness for the fluctuations of the synoptic-scale specific humidity at 850 hPa (a, b) and 400 hPa (c, d) for January (a, c) and July (b, d).

A marked decrease, as compared to the lower troposphere, in the area occupied by the tropical-type pattern of $S_{q'}$ at 400 hPa (cf. Fig. 5a–d) evidently is associated with a decrease in the water vapour availability and the latent heating at this level in the tropics, accompanied by a much lower intensity of the water vapour transport at high levels by predominantly lower-tropospheric tropical synoptic-scale systems (Hsu, 2005).

Figure 6a–d illustrates the geographic distribution of the standardized skewness for the synoptic-scale specific humidity $S_{st,q'}$ at the same atmospheric levels for January and July. The comparison of Figs. 5a–d and 6a–d shows that there exists a statistically significant divergence, in terms of skewness, of a sampled stochastic process of the synoptic-scale specific humidity from Gaussian process in all the discussed above regions with high values of $S_{q'}$, inasmuch as the absolute values of $S_{st,q'}$ in those regions are larger than 2.

3.1.4. Zonal and meridional winds. Our analysis revealed statistically significant non-standardized skewnesses for zonal wind $S_{u'}$ and meridional wind $S_{v'}$ only at 850 hPa (see Fig. 7a–f). Zonal velocity is skewed negatively at this pressure level in the regions of the mid-latitude cyclonic eddy generation in both Hemispheres (Fig. 7a and b). Meridional velocity is skewed positively (negatively) in the same regions of the Northern (Southern) Hemisphere (Fig. 7c and d). The magnitudes of both $S_{u'}$ and $S_{v'}$ amount about (0.3–0.6) in the indicated locations. A tendency to the change in sign of $S_{u'}$ and $S_{v'}$ can be traced in the areas of the mid-latitude cyclolysis, as compared to the locations of their generation. In all the aforementioned regions non-zero skewnesses for horizontal wind components are statistically significant only in the winter Hemispheres. By and large the meridional velocity exhibits rather natural, close-to-the-antisymmetric about the equator, overall structure of skewness (see Fig. 7c and d). Well-marked belts of high positive values of $S_{u'}$ are observed in the subtropics of the SH for both January and July, and in the subtropics of the NH for January. These results are in agreement with those obtained by Monahan (2006a,b) for the surface winds. In the tropics, the zonal wind skewness is patchy for January and July in both Hemispheres. In the Southeast Asian and Indian monsoon systems, the zonal wind skewness has markedly negative values for July, which points, first, to the robustness of the basic mechanism for the summer monsoon generation which is built on the ocean-to-land temperature difference and, secondly, to a rather strong deviation of the statistics for the principally ageostrophic monsoon winds from Gaussian statistics. Fig. 7e and f illustrate the non-standardized skewnesses at 850 hPa, respectively, for zonal wind $S_{u'}$ in the region of the North Atlantic storm track for January and meridional wind $S_{v'}$ in the location of the South Pacific storm track for July.

Figure 8a–d depicts the geographic distributions of the standardized skewness for the synoptic-scale zonal $S_{st,u'}$ (Fig. 8a and b) and meridional $S_{st,v'}$ (Fig. 8c and d) velocities at 850 hPa. The comparison of Figs. 7a–d and 8a–d reveals that there exists a statistically significant departure, in terms of skewness, of a sampled stochastic processes of the synoptic-scale zonal and

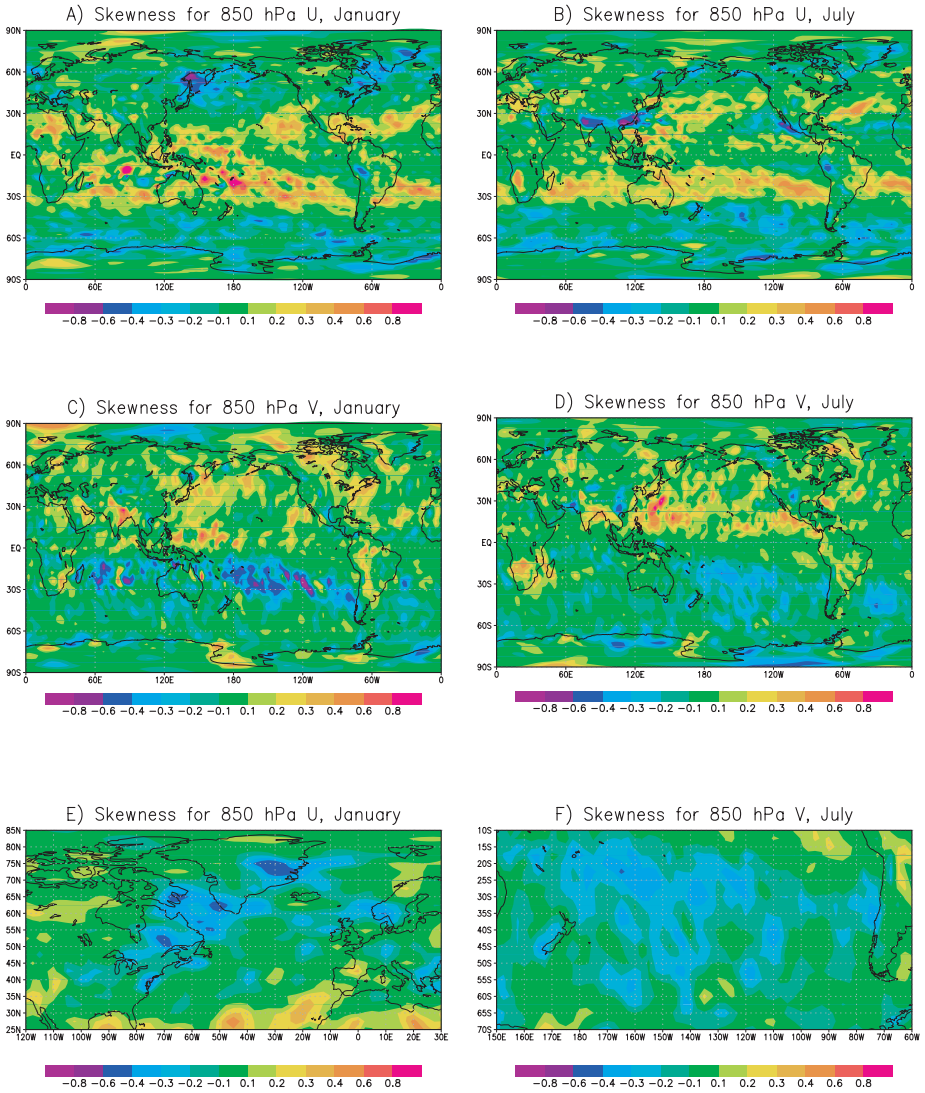

Fig. 7. Skewness at 850 hPa for the synoptic-scale fluctuations of zonal (a, b) and meridional (c, d) wind and the zoomed plots for 850 hPa of the zonal wind in the North Atlantic (e) and of the meridional wind in the South Pacific (f) for January (a, c, e) and July (b, d, f).

meridional winds from a Gaussian process in all the discussed above regions with high values of $S_{u'}$ and $S_{v'}$, since the absolute values of $S_{st,u'}$ and $S_{st,v'}$ in those regions are larger in magnitude than 2.

In our paper, we do not analyse the synoptic-scale vorticity skewness $S_{\zeta'}$. The field of $S_{\zeta'}$ (not shown in the paper) appears to be much more patchy, as compared to $S_{\omega'}$, $S_{u'}$ and $S_{v'}$ fields, which makes it doubtful the estimation of the statistical significance of the deviation of the synoptic-scale vorticity from the Gaussian process. This is because the initial ERA40 reanalysis data on the vorticity are rather noisy and reflect much more small-scale features than those on the horizontal winds (Bengtsson et al., 2004b). For that reason, the cyclone/anticyclone asymmetry, as an example, which is expected to be well traced by $S_{\zeta'}$, is actually not distinctly followed by this field, as opposed to $S_{\omega'}$.

3.1.5. Summary of the results on skewness of the synoptic-scale variations. The comparison of Figs. 1a, b, 3a, b, 5a, b and 7a, b clearly points to dissimilar geographic patterns for the skewnesses of the synoptic-scale vertical velocity, temperature, specific humidity, and horizontal winds. This, in particular, casts some doubts upon the occurrence of the universal spacial scale for the synoptic eddies (and the accompanying baroclinic zones), for all the discussed above variables, specifically in the atmosphere with different moisture content in different regions.

In the foregoing, we discussed some probable reasons for non-Gaussianity of the synoptic-scale skewnesses of the considered variables. However, we can by no means exclude the alternative explanations for a non-Gaussian character of the free-troposphere synoptic component. We have already mentioned a

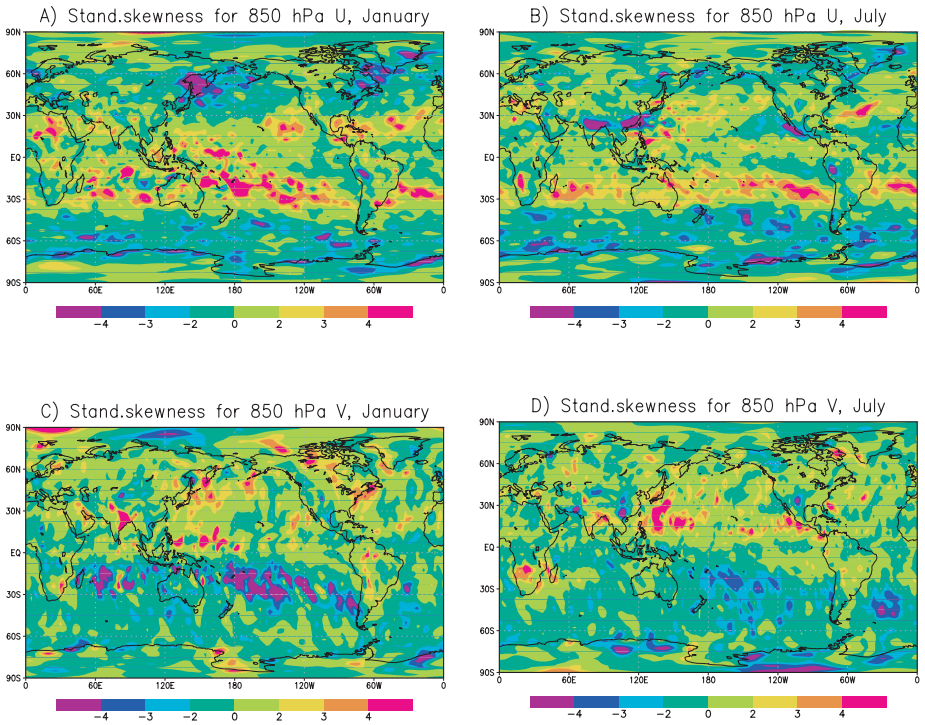

Fig. 8. Standardized skewness at 850 hPa for the synoptic-scale fluctuations of zonal (a, b) and meridional (c, d) wind for January (a, c) and July (b, d).

displacement in the storm-track positions as a feasible reason for the high values of the synoptic-scale vertical velocity skewness in the mid-latitude storm tracks. Furthermore, as is shown in Holzer (1996), the high values of skewness for the synoptic fluctuations of the geopotential height Φ can be attributed to the rectification of near-symmetric velocity fluctuations by the advective non-linearity.

We note also that a variety of physical mechanisms may stand behind the discussed above phenomenological structure of the skewness distributions. Examples are the non-linear wave-wave interaction at the growth stage of the baroclinic eddies Farrell (1982, 1984), a multiplicative noise from the unresolved components of different nature (e.g. originating from the mesoscale moist processes in the atmosphere) (Sura et al., 2005), and the difference between moist and dry static stabilty (Lapeyre and Held, 2004). Also, an intense latent heat release within concentrated synoptic vortices is one of the basic reasons for the above-mentioned high non-linearity and spatial inhomogeneity inherent in the ensembles of synoptic systems in the moist atmosphere (Lapeyre and Held, 2004). In this connection, physical mechanisms should be mentioned, which can generate the cyclone/anticyclone asymmetry (and finally, bring about different signs of the synoptic-scale skewnesses over different regions). These are the non-linear geostrophic adjustment (Kuo and Polvani, 2000), the frontogenesis at the tropopause and the forward cascade of tropopause potential temperature variance (Hakim et al., 2002), the high-magnitude latent heat release resulting in the linkage between the low-level vorticity and moisture, due to the correlated horizontal transports of these quantities (Zhang and Held, 1999; Lapeyre and Held, 2004), and the cyclone/anticyclone vortex-merger asymmetry at the tropopause (Hakim and Canavan, 2005). It is pertinent to note here that the asymmetry of the surface drag law with respect to a (non-zero) mean state is suggested in (Monahan, 2004) as a reason for a skewed probability density function for near-surface winds.

Let us notice, with respect to the existing controversy in the literature regarding the statistical significance of skewness for the basic synoptic-scale fields, that the obtained in our paper results of calculations of $S_{\omega'}$ at 500 hPa (see Fig. 1c and d) do not in fact contradict the demonstrated in Weaver and Ramanathan (1997) close-to-Gaussian distributions for the vertical velocity fluctuations at the aforementioned atmospheric level over the entire North Pacific and North Atlantic storm tracks for January and July of 1985–1989. Being averaged over the indicated storm tracks the calculated in the present paper values for the magnitude of $S_{\omega'}$ at 500 hPa are statistically insignificant for both January and July. We note also that our results concerning the spatial distribution of skewness for the synoptic-scale temperature fluctuations $S_{T'}$ within the lower-tropospheric portion of the North Pacific storm track in winter (Fig. 3a) are in a good agreement with the findings of Swanson and Pierrehumbert (1997), who reported on the positive (negative) skewness for the indicated variable at the upstream (downstream) end of the mentioned storm track in that season.

In so far as the synoptic-scale fluctuations for any one of the variable studied in this paper are significantly skewed, in particular, in the locations of the mid-latitude storm tracks, one cannot treat these fluctuations as one-dimensional Gaussian processes. Moreover, in that case the totality of the synoptic-scale variations cannot be viewed as a multidimensional Gaussian process, as for this latter process all the partial distributions must be one-dimensional Gaussian processes (Feller, 1971). As a result, one may expect to obtain significantly non-zero values for the third-order moments (TOMs) in the aforementioned locations. The more so that the third-order moments (TOMs) and the discussed above triple correlations of a single variable are very different quantities because TOMs involve gradients. As is well known from the theory of turbulence the non-Gaussian statistics can evolve in the case of isotropic turbulence for the fields associated, for example, with pressure fluctuations and vorticity spottiness (Chen et al., 1989). In this, although the velocity fluctuations are Gaussian in the indicated case, the skewness of a velocity gradient perturbations is non-zero and can be related to the energy dissipation rate and the spectral flow of energy (McComb, 1992). TOMs are considered at length in the next two subsections.

We note also that, even though statistical insignificance of synoptic-scale skewness is revealed in one or another location, this may be due to a short sample length. We have tested this hypothesis by recomputing skewnesses for the entire boreal winter (DJF) and summer (JJA), rather than for separate months. By and large the plots for the DJF and JJA skewnesses of the bandpass-filtered synoptic-scale variations (not shown in this paper) look very similar to those for January and July, respectively. Hence we conclude that the revealed by our analysis insignificance of skewness in one or another site is not due to an inadequate sample length.

3.2. *Contribution from the third-order moments to the synoptic-scale kinetic energy tendency*

A non-negligible role of the third-order moments in the synoptic-scale dynamics can be illustrated by the example of the equation for the synoptic-scale kinetic energy E_s in p-coordinate within the hydrostatic approximation. In this, the complete system of the hydrodynamic eqauations written in the above-mentioned approximation is used as the initial set of equations (see Lorenz, 1967), which gives

$$\frac{\partial \overline{E_s}}{\partial t} = -\overline{\vec{V}} \cdot \nabla^p \overline{E_s} - \overline{\vec{V}' \cdot \nabla^p E_s} - \overline{u'\vec{V}'} \cdot \nabla^p \overline{u} - \overline{v'\vec{V}'} \cdot \nabla^p \overline{v} + \frac{\tan\phi}{a}\left(\overline{u'^2}\,\overline{v} - \overline{u'v'}\,\overline{u}\right) + f\overline{u'_g v'_{ag}} - f\overline{v'_g u'_{ag}} + \overline{u'F'_\lambda} + \overline{v'F'_\phi}. \quad (1)$$

Here t is time, p is pressure, $E_s = (1/2)(u'^2 + v'^2)$, $\vec{V} = (u, v, \omega)$, F_λ and F_ϕ is the zonal and the meridional component of the small/meso-scale friction force, respectively, f is the Coriolis parameter, $u'_{g(ag)}$ and $v'_{g(ag)}$ is, correspondingly, the geostrophic (ageostrophic) component of the synoptic-scale zonal and meridional wind, $\nabla^p = (\nabla_\lambda, \nabla_\phi, \nabla_p)$ is the gradient operator, with $\nabla_\lambda = (1/a\cos\phi)\partial/\partial\lambda$, $\nabla_\phi = (1/a)\partial/\partial\phi$ and $\nabla_p = \partial/\partial p$, where a is the Earth's radius. The bar above each term in eq. (1) denotes a time averaging of the corresponding term over the total (combined) set of the same calendar months from 1976 to 2002. In this, the combined daily (or 6-hourly) array of the ERA40 reanalysis data on any variable X for a given calendar month, once processed with the Murakami bandpass filter, is used as the synoptic-scale input 'data', X', in the relevant terms of the eq. (1). Let us notice that the overbar in the eq. (1) is conventionally assumed to commute with the time derivative.

Previously, the equation for $\overline{E}_s$ has been studied, for example, by Kurihara (1970) and Lau (1979). However, the forms of the $\overline{E}_s$-equation in those papers differ from (1). Kurihara (1970) has investigated only the equation for the zonally averaged $\overline{E}_s$, in accordance with the zonal formulation of his model. Lau (1979), in turn, has studied a non-zonal version of this equation but he has neglected the contribution from the vertical motions. In this latter paper, it was shown, in particular, that the contribution from the third-order moments is non-negligible. In our study, we use a more general eq. (1) for $\overline{E}_s$, as compared to Kurihara (1970) and Lau (1979). Nonetheless, we do not take into account the terms $f\overline{u'_g v'_{ag}}$ and $f\overline{v'_g u'_{ag}}$ including the ageostrophic component of the synoptic-scale eddy motions in this equation, for two reasons. First, as shown in (Opsteegh and van den Dool, 1979), this group of terms in the equation for $\overline{E}_s$ contains very large (up to 100 per cent) errors once estimated on the basis of the observational or empirical data, which could be brought about, in particular, by the calculations of the correlations comprising the synoptic-scale gradients of Φ'. Secondly, our goal is to compare the contributions from the third-order moments and the second-order moments to the equation for $\overline{E}_s$, merely at the level of the order of magnitude. For the same reasons we do not analyse in this paper the contribution to the synoptic-scale eddy kinetic energy E_s from the friction terms $\overline{u'F'_\lambda}$ and $\overline{v'F'_\phi}$.

The third-order moments enter the equation for the synoptic-scale eddy kinetic energy (1) in the form

$$M_{E,3} = -\overline{\vec{V}'_H \cdot \nabla_H E_s} - \overline{\omega' \partial E_s/\partial p}, \quad (2)$$

where $\vec{V}'_H$ and ∇_H is the vector of the synoptic-scale horizontal velocity and the horizontal gradient operator, respectively.

Figure 9 displays the $M_{E,3}$ field, together with

$$M_{E,2} = -\overline{\vec{V}} \cdot \nabla^p \overline{E_s} - \overline{u'\vec{V}'} \cdot \nabla^p \overline{u} - \overline{v'\vec{V}'} \cdot \nabla^p \overline{v} + \frac{\tan\phi}{a}\left(\overline{u'^2}\,\overline{v} - \overline{u'v'}\,\overline{u}\right) \quad (3)$$

(the latter represents the contribution from SOMs to eq. 1), at 850 and 700 hPa pressure levels for the NH and the SH winters.

As seen from Fig. 9, the contribution from TOMs to the equation for $\overline{E}_s$ is generally non-negligible in winter. While the patterns of the third-order moments are more localized than those of the second-order moments, the characteristic magnitudes of

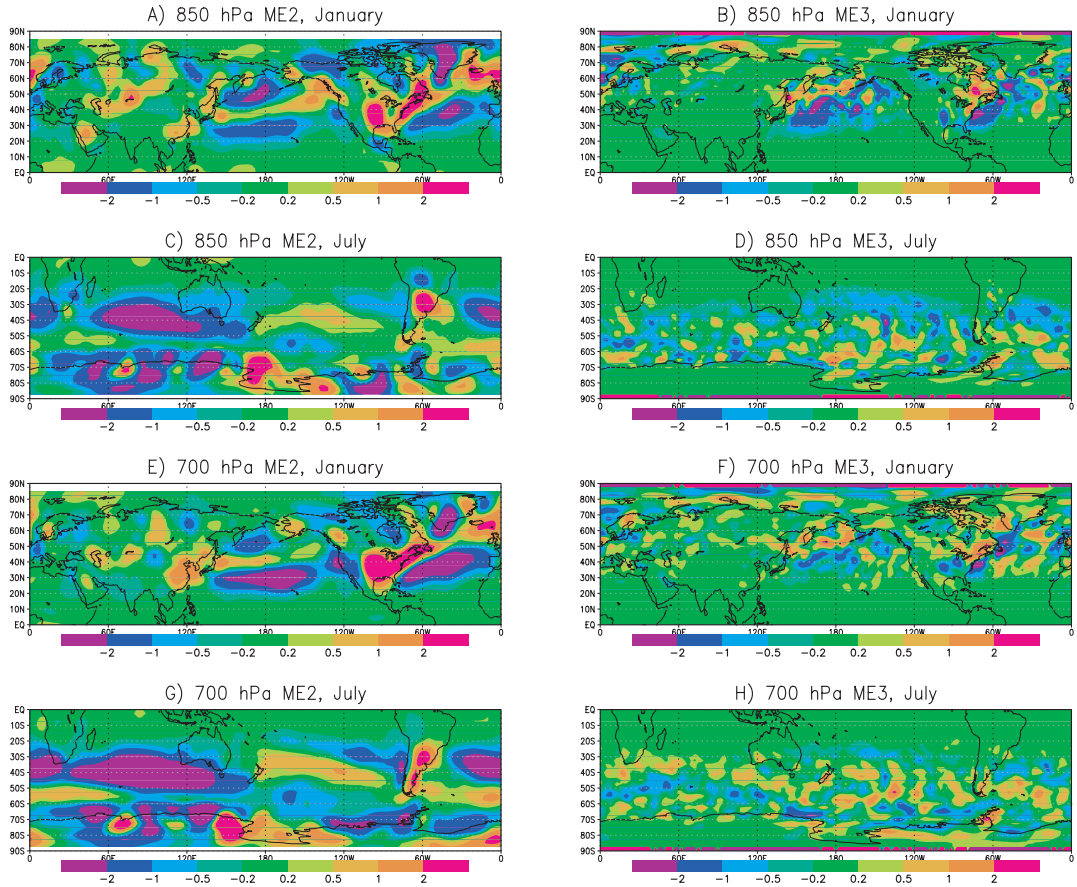

Fig. 9. Geographic distributions for the second-order $M_{E,2}$ (a, c, e, g) and the third-order $M_{E,3}$ (b, d, f, h) synoptic moments (both in 10^{-5} m^2 s^{-3}) in the equation for the synoptic-scale kinetic energy $\overline{E}_s$ in winter, at 850 hPa for the NH (a, b) and the SH (c, d), and at 700 hPa for the NH (e, f) and the SH (g, h)

the former are at least one-tenth those of the latter. Generally, $M_{E,3}$ peak near the regions of synoptic storm generation. These regions have been detected and shown in (Hoskins and Hodges, 2002, 2005; Trigo, 2006). We note that in the middle troposphere of both Hemispheres (specifically in the SH), $M_{E,3}$ reveal a wavy shape in the storm track regions. This wavy shape is similar to that observed and modelled for the ageostrophic fluxes during the synoptic-scale eddy life cycle (Wallace et al., 1988; Chang, 1993; Chang and Orlanski, 1993; Orlanski and Gross, 2000).

Figure 10 illustrates the contribution to $M_{E,3}$ from the individual third-order moments. Namely, it demonstrates the geographic distribution in the NH of the term associated with the combined horizontal self-advection of the synoptic-scale kinetic energy E_s by the zonal and meridional synoptic-scale motions (the first term in the right side of eq. 2). According to the results of our calculations, the most marked contribution of TOMs to the eq. (1) for E_s comes just from this term, while the TOMs induced by the metric terms in the original equations, and specifically the TOM associated with the vertical advection of the above-mentioned variable by the synoptic-scale motions, are of much less importance. For that reason, only the horizontal self-advection TOM is shown in Fig. 10. The positions of the storm track axes, in which the synoptic-scale kinetic energy reaches its maxima (Oort, 1983; Peixoto and Oort, 1992) and the corresponding horizontal gradient passes zero value, are well marked in Fig. 10 (especially in the lower troposphere) as the geometric loci of the divides between the positive and negative values of $-\overline{\vec{V}'_H \cdot \nabla_H E_s}$.

3.3. *Contribution from the third-order moments to the meridional heat and moisture fluxes*

In addition to the equation for $\overline{E}_s$, we analysed the equations for the synoptic-scale meridional fluxes of heat $\overline{v'T'}$ and moisture $\overline{v'q'}$. The fluxes $\overline{v'T'}$ and $\overline{v'q'}$ have to be parametrized in most of the EMICs, as well as in the statistical-dynamical and energy-moisture balance climate models.

In p-coordinate and the same hydrostatic approximation the equations for $\overline{v'T'}$ and $\overline{v'q'}$ in non-divergent form read

$$\frac{\partial \overline{v'X'}}{\partial t} = M_{X,2} + M_{X,3} + \overline{v'Q'_X} + \overline{X'F'_\phi} - f\overline{u'_{ag}X'}, \qquad (4)$$

where $X = T, q$, and Q'_X denotes the synoptic-scale sources/sinks of heat (for $X = T$) and moisture (for $X = q$). In the present

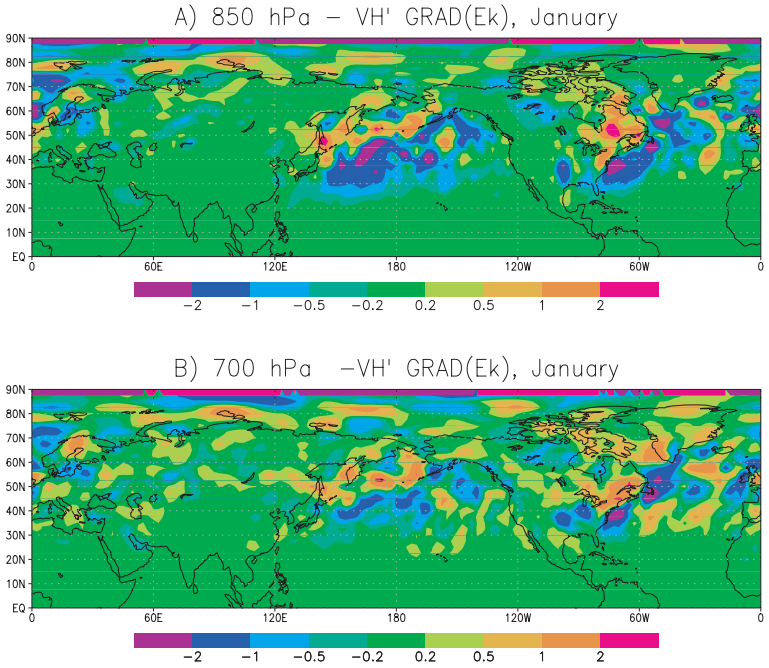

Fig. 10. Geographic distributions in the NH for the $-\overline{\vec{V}'_H \cdot \nabla_H E_s}$ term (in 10^{-5} m^2 s^{-3}) entering $M_{E,3}$ (see eq. 2) at 850 hPa (a) and at 700 hPa (b), for January.

paper, we do not deal with the attributed to these sources/sinks synoptic-scale moments represented by the third term in the right side of the last equation, as well as with the last two terms in its right side, which describe the contribution to the $\overline{v'X'}$ fluxes from the atmospheric friction and the ageostrophic synoptic-scale motions. The $M_{T,2}$, $M_{T,3}$ and $M_{q,2}$, $M_{q,3}$ terms, which are hereafter referred to, respectively, as the second- and the third-order synoptic moments in the corresponding equations for $\overline{v'T'}$ and $\overline{v'q'}$, can be written as follows

$$M_{T,2} = -\overline{\vec{V}} \cdot \nabla^p \overline{v'T'} - \overline{v'\vec{V}'} \cdot \nabla^p \overline{T} - \overline{T'\vec{V}'} \cdot \nabla^p \overline{v} - 2a^{-1} \tan\phi \overline{u}\,\overline{u'T'} + (R\overline{T}/c_p p)\overline{v'\omega'} + (R\overline{\omega}/c_p p)\overline{v'T'} \quad (5)$$

$$M_{T,3} = -\overline{\vec{V}'_H \cdot \nabla_H v'T'} - \overline{\omega'\partial v'T'/\partial p} - a^{-1} \tan\phi \overline{u'^2 T'} + (R/c_p p)\overline{v'\omega'T'}, \quad (6)$$

where R and c_p are the gas constant and the specific heat at constant pressure for the atmospheric air, and

$$M_{q,2} = -\overline{\vec{V}} \cdot \nabla^p \overline{v'q'} - \overline{v'\vec{V}'} \cdot \nabla^p \overline{q} - \overline{q'\vec{V}'} \cdot \nabla^p \overline{v} - 2a^{-1} \tan\phi \overline{u}\,\overline{u'q'} \quad (7)$$

$$M_{q,3} = -\overline{\vec{V}'_H \cdot \nabla_H v'q'} - \overline{\omega'\partial v'q'/\partial p} - a^{-1} \tan\phi \overline{u'^2 q'}. \quad (8)$$

Similar equations, but with the omitted terms including the third-order moments, have been used in (Handorf et al., 1999; Petoukhov et al., 2003). As was shown in the former paper, an implementation of the prognostic equation for $\overline{v'T'}$ improves the results of the climate simulations, as compared to the diagnostic scheme for this flux.

The terms $M_{T,2}$ and $M_{T,3}$ in the equation for $\overline{v'T'}$ at 700 hPa in the Northern Hemisphere for January are shown, respectively, in Fig. 11a and b. As seen from Fig. 11a and b, the contribution from TOMs to the prognostic equation for $\overline{v'T'}$ is not negligible: in the winter storm tracks, $M_{T,3}$ ranges up to 10–15 per cent of $M_{T,2}$. In the equation for $\overline{v'q'}$, the relative role of TOMs is somewhat higher for the lower troposphere of the NH in winter (see Fig. 12a and b), where locally $M_{q,3}$ attains about one-third $M_{q,2}$. In this, the contribution from TOMs to $\overline{v'T'}$ and $\overline{v'q'}$ is larger in the North Atlantic storm track relative to that in its North Pacific counterpart.

In the Northern Hemisphere summer, the role of the third-order moments in the equations for $\overline{v'T'}$ and $\overline{v'q'}$ (not shown in this paper) dramatically diminishes, as compared to the Northern Hemisphere winter, although TOMs still remain on the verge of detection in the north Atlantic storm track. This is consistent with the conclusion reached in the previous section on the increase of the deviations from Gaussianity in the regions with higher intensity of the synoptic-scale fluctuations.

We analysed the role of the individual third-order moments in the $M_{T,3}$ and $M_{q,3}$ terms for the NH. The most marked contribution of TOMs to the prognostic equations for the synoptic-scale meridional fluxes of heat and moisture comes from the advection of these variables by the horizontal synoptic-scale motions $-\overline{\vec{V}'_H \cdot \nabla_H v'T'}$ (Fig. 11c) and $-\overline{\vec{V}'_H \cdot \nabla_H v'q'}$ (Fig. 12c) respectively. The TOMs arising from the metric terms, and specifically the TOMs associated with the vertical advection of the above-

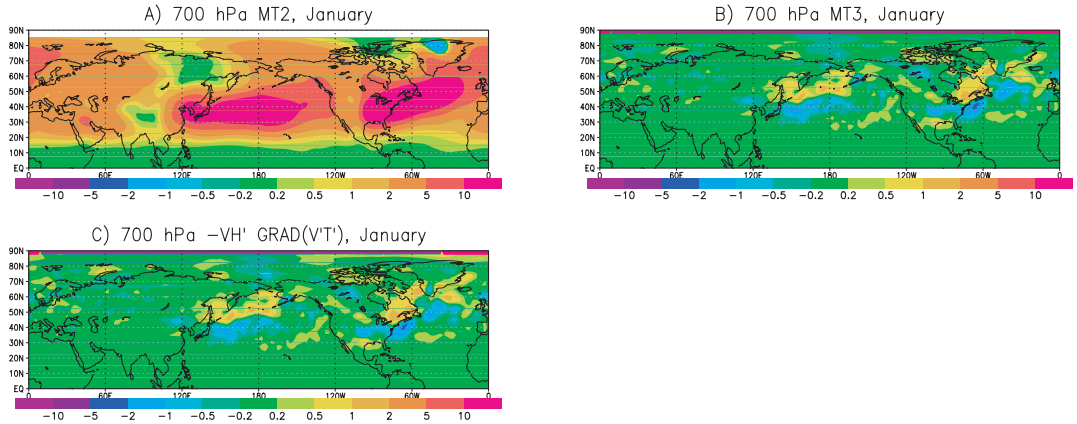

Fig. 11. Geographic distributions, in the NH, for the second-order synoptic moments $M_{T,2}$ (a), the third-order synoptic moments $M_{T,3}$ (b) and for the horizontal self-advection term $-\overline{\vec{V}'_H \cdot \nabla_H v'T'}$ (c) (all in 10^{-5} K m s^{-2}), in the equation for the meridional component of the synoptic-scale sensible heat flux (see eqs. 4–6), at 700 hPa for January.

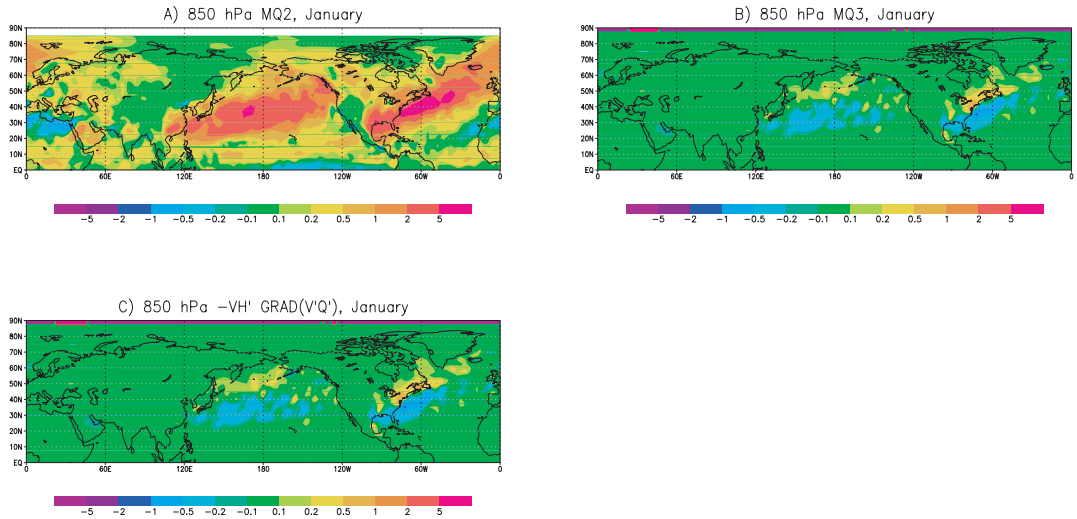

Fig. 12. Geographic distributions, in the NH, for the second-order synoptic moments $M_{q,2}$ (a), the third-order synoptic moments $M_{q,3}$ (b) and for the horizontal self-advection term $-\overline{\vec{V}'_H \cdot \nabla_H v'q'}$ (c) (all in 10^{-8} m s^{-2}), in the equation for the meridional component of the synoptic-scale latent heat flux (see eqs 4, 7 and 8), at 850 hPa for January.

mentioned variables by the synoptic-scale motions are of much less importance.

As in the case of E_s (cf. Fig. 10a and b), the positions of the storm track axes (specifically that associated with the Gulf Stream), in which the meridional synoptic-scale fluxes of sensible and latent heat reach their maxima (Oort, 1983; Peixoto and Oort, 1992) and the corresponding horizontal gradients pass zero values, are well marked, respectively, in Figs. 11c and 12c as the geometric loci of the divides between the positive and negative values, correspondingly, of $-\overline{\vec{V}'_H \cdot \nabla_H v'T'}$ and $-\overline{\vec{V}'_H \cdot \nabla_H v'q'}$.

In the austral winter, $M_{T,3}$ and $M_{q,3}$ in the SH (not shown in the paper) are slightly less structured as against their NH counterparts in the boreal winter, whereas the magnitudes of $M_{T,3}$ and $M_{q,3}$ in the SH appear to be closely allied to those in the NH, within the storm track areas. In the austral summer, $M_{T,3}$ and $M_{q,3}$ are small in the SH.

4. Conclusions

In this paper, skewnesses for the (2.5–6) d bandpass-filtered synoptic fluctuations of vertical velocity, temperature, the specific humidity and horizontal winds are calculated, based on the ERA40 reanalysis data for 1976–2002. Additionally, the contributions from the third-order moments to the tendency equations for the synoptic-scale kinetic energy and the synoptic-scale meridional fluxes of heat and moisture are estimated.

Generally skewnesses for the synoptic fluctuations of the above-mentioned variables differ significantly from the Gaussian

(zero) value. High values of skewnesses are observed mostly in the locations of the mid-latitude cyclogenesis. For the negatively skewed vertical velocity and positively skewed temperature, non-Gaussianity is revealed throughout the total troposphere in these regions, where the typical values of $S_{\omega'}$ and $S_{T'}$ are about $-(0.6–0.8)$ and $+(0.3–0.6)$, respectively. As to the synoptic-scale fluctuations of the specific humidity, these are by and large skewed positively in the polar regions and in the mid-latitude storm tracks (with $S_{q'}$ about $+(0.6–0.8)$ or even larger there) and negatively—in the lower troposphere of the tropics. A statistically significant skewness for horizontal winds is found only in the lower troposphere, again mainly in the regions of the synoptic-scale cyclogenesis. In those locations, zonal wind is skewed negatively. The meridional wind skewness differs in the Northern and Southern Hemispheres, where it is predominantly positive and negative, respectively. For both zonal and meridional winds, the magnitude of the non-standardized skewness reaches 0.4.

The analysed results attest that the high values of skewnesses for the vertical velocity, temperature and the specific humidity are not only a signature of the underlying non-linearity of the synoptic processes, for example, in the locations of the mid-latitude storm tracks, but they may also serve as an indicator for the important large-scale quasi-stationary non-linear structures of the atmospheric circulation (such as the monsoon systems, the quasi-permanent centres of action and the ITCZ), as well as the cyclone/anticyclone asymmetry inherent in the synoptic component of the atmospheric motions.

The strongest deviations from Gaussianity are revealed for the specific humidity and vertical velocity, as compared to all the other studied variables. Such situation is quite different from the observed for small-scale turbulence in the atmospheric convective boundary layer, where, for instance, the potential temperature is skewed stronger than the vertical velocity (Gryanik and Hartmann, 2002). This result is in accord with the above-mentioned findings of Nakamura and Shimpo (2004).

Our estimates of the contribution from the third-order moments (TOMs) to the equation for the synoptic eddy kinetic energy $\overline{E}_s$ demonstrate a non-negligible role of TOMs in the regions of the synoptic-scale cyclogenesis. A significant contribution from the third-order moments to the eddy kinetic energy in the cyclogenesis areas is consistent with our results regarding significantly non-zero skewnesses in those regions.

We also estimated the contribution from TOMs to the prognostic equations for the synoptic-scale meridional fluxes of sensible heat and moisture. Generally the indicated TOMs are non-negligible in the Northern Hemisphere storm tracks during the boreal winter. For the Southern Hemisphere winter, the contribution from TOMs is also non-negligible and appears to be closely allied to that in the NH, in the storm tracks, although the patterns of high values of TOMs are somewhat more patchy in the SH. In the boreal summer, TOMs entering the aforementioned prognostic equations are detectable in the NH only for the North Atlantic storm track. In the austral summer, TOMs are small in the prognostic equations for the synoptic-scale meridional fluxes of sensible and latent heat in the SH.

We did not aim in this paper at the development of parametrizations for the synoptic processes. Nonetheless, the presented results can be useful for validating the synoptic-scale statistics produced by the low-order stochastic models of the atmospheric dynamics and climate (see, e.g. Majda et al., 2001; Achatz and Opsteegh, 2003; Franzke et al., 2005) and GCMs, as well as for developing and testing statistical-dynamical climate models and EMICs. Also, the studied triple correlations are among the direct indicators of non-linearity of the atmospheric processes.

Let us note in closing that, as is clear from the obtained results, a sign of skewness for a synoptic-scale fluctuation of a given variable over the extended regions with high synoptic activity by and large correlates with a sign of this fluctuation developed in the interior of the spatial substructures (a) (i.e. within the concentrated synoptic vortices with relatively small fractional area) in the ensembles of the representative (dominant) for those regions synoptic systems. In view of this, we can hypothesize that strong non-linearity and significant spatial inhomogeneity (high internal structuredness) inherent in the synoptic systems can be the intrinsic reason for the revealed by our analysis markedly non-zero skewnesses (non-Gaussianity) of the synoptic-scale stochastic fields in the indicated regions. In this, an 'index of structuredness', $E_{\mathrm{fc},X'}$, can be introduced as an integral measure for the mentioned non-linearity and spatial inhomogeneity. We can define $E_{\mathrm{fc},X'}$ as the difference between a 'symmetric' fractional area $A_m(=1/2)$ inherent in the non-structured on the considered spatial-temporal scales stochastic field, and the actual fractional area $A_{+,X'}$ occupied by the positive values of a spatially distributed stochastic field X', which is regulated by the ensemble of the representative for a given region synoptic systems. In this, $S_{X'}$ may highly correlate with $E_{\mathrm{fc},X'}$, so that a zero value of $E_{\mathrm{fc},X'}$ corresponds to a zero value of $S_{X'}$, and $S_{X'}$ monotonically increases with the increase in $E_{\mathrm{fc},X'}$. We note, in support of our hypothesis, that the bulk of the analysed in our paper peculiarities of the geographic, vertical and seasonal distributions of skewnesses for the synoptic-scale fields can be interpreted, at least in a qualitative sense, in terms of $E_{\mathrm{fc},X'}$. In particular, the transitions from the regions of the substantially cyclonic activity with high positive values for $S_{w'}$ to those of the mainly anticyclonic one with $S_{w'} < 0$ in the middle latitudes of both Hemispheres can be traced by the corresponding to these transitions change in sign of $E_{\mathrm{fc},w'}$. From this point of view the mid-latitude free troposphere can bear similarities to the mid-latitude planetary boundary layer. The latter demonstrates for the convective conditions a high correlation between, for example, S_w and the ensemble-mean fractional area $A_{+,w}$ occupied by the positive values of the spatially distributed field of w (Randall et al., 1992; Gryanik and Hartmann, 2002). Further studies are needed, of course, to provide careful quantitative checking of our hypothesis for the profound linkage between $E_{\mathrm{fc},X'}$ and $S_{X'}$

for all the synoptic-scale fields of the free troposphere analysed in the present paper.

5. Acknowledgements

We are indebted to V.M. Gryanik for useful discussions on the topic of the manuscript. Valuable comments on earlier versions of this work by the anonymous reviewers are gratefully acknowledged. The presented figures are produced with the use of the GrADS software developed at the Center for Land-Ocean-Atmosphere Studies. This work has been supported by the President of Russia grant 4166.2006.5, and by the research programs by Russian Academy of Sciences and by the Russian Ministry for Education and Science (Rosnauka).

References

Abramowitz, M. and Stegun, I. 1972. *Handbook of Mathematical Functions and Formulas, Graphs and Mathematical Tables*, Dover, New York.

Achatz, U. and Opsteegh, J. D. 2003. Primitive-equation based low-order model with seasonal cycle. Part I: model construction. *J. Atmos. Sci.* **60**, 465–477.

Balasubramanian, G. and Yau M. K. 1996. The life cycle of a simulated marine cyclone: energetics and PV diagnostics. *J. Atmos. Sci.* **53**, 639–653

Bengtsson, L., Hagemann, S. and Hodges, K. I. 2004. Can climate trends be calculated from reanalysis data? *J. geophys. Res.* **109**, D11111.

Bengtsson, L., Hodges, K. I. and Hagemann, S. 2004. Sensitivity of the ERA40 reanalysis to the observing system: determination of the global atmospheric circulation from reduced observations. *Tellus* **56A**, 456–471.

Blackmon, M. 1976. A climatological spectral study of the 500 mb geopotential height of the Northern Hemisphere *J. Atmos. Sci.* **33**, 1607–1623.

Bograd, S., Schwing, F., Mendelssohn, R. and Green-Jessen, P. 2002. On the changing seasonality over the North Pacific. *Geophys. Res. Lett.* **29**, 1333.

Branscome, L. 1983. A parameterization of transient eddy heat flux on a beta-plane. *J. Atmos. Sci.* **40**, 2508–2521.

Branstator, G. 1995. Organization of stormtrack anomalies by recurring low-frequency circulation anomalies. *J. Atmos. Sci.* **52**, 207–226.

Bromwich, D. H. 1991. Mesoscale cyclogenesis over the southwestern Ross Sea linked to strong katabatic winds. *Mon. Wea. Rev.* **119**, 1736–1752.

Chang, E. 1993. Downstream development of baroclinic waves as inferred from regression analysis. *J. Atmos. Sci.* **50**, 2038–2053.

Chang, E. and Orlanski, I. 1993. On the dynamics of a storm track. *J. Atmos. Sci.* **50**, 999–1015.

Chen, H., Herring, J. R., Kerr, R. M. and Kraichnan, R. H. 1989. Non-Gaussian statistics in isotropic turbulence. *Phys. Fluids A* **1**, 1844–1854.

Chen, P., Hoerling, M. P. and Dole, R. M. 2001. The origin of the subtropical anticyclones. *J. Atmos. Sci.* **58**, 1827–1835

Christoph, M., Ulbrich, U. and Haak, U. 1995. Faster determination of the intraseasonal variability of storm tracks using Murakami's recursive filter. *Mon. Wea. Rev.* **123**, 578–581.

Claussen, M., Mysak, L., Weaver, A., Crucifix, M., Fichefet, T. and co-authors. 2002. Earth system models of intermediate complexity: closing the gap in the spectrum of climate system models. *Clim. Dyn.* **18**, 579–586.

Cohen, J., Saito, K. and Entekhabi, D. 2001. The role of the Siberian High in the Northern Hemisphere climate variability. *Geophys. Res. Lett.* **28**, 299–302.

Corte-Real, J., Qian, B. and Xu, H. 1998. Regional climate change in Portugal: precipitation variability associated with large-scale atmospheric circulation. *Int. J. Climatol.* **18**, 619–635.

Davis, R. E., Hayden, B. P., Gay, D. A., Phillips, W. L. and Jones, G. V. 1996. The North Atlantic subtropical anticyclone *J. Climate* **10**, 728–744

Defant, A. 1921. Die Zirkulation der Atmosphäre in den gemässigten Breiten der Erde. *Geogr. Ann.* **3**, 209–266.

Eckhardt, S., Stohl, A., Wernli, H., James, P., Forster, C., and co-authors. 2004. A 15-year climatology of warm conveyor belts. *J. Climate* **17**, 218–237.

Egger, J. 1975. A statistical-dynamical model of the zonally averaged steady-state of the general circulation of the atmosphere. *Tellus* **27**, 325–350.

Fantini, M. 2004. Bariclinic instability of a zero-PVE jet: enhanced effects of moisture on the life cycle of midlatitude cyclones. *J. Atmos. Sci.* **61**, 1296–1307.

Farrell, B. 1982. The initial growth of disturbances in a baroclinic flow. *J. Atmos. Sci.* **39**, 1663–1686.

Farrell, B. 1984. Modal and non-modal baroclinic waves. *J. Atmos. Sci.* **41**, 668–673.

Farrell, B. and Ioannou, P. 1994. A theory for the statistical equilibrium energy spectrum and heat flux produced by transient baroclinic waves. *J. Atmos. Sci.* **51**, 2685–2698.

Feller, W. 1971. *An Introduction to Probability Theory and Its Applications* Volume 2, Wiley, New York.

Fitch, M. and Carleton, A. M. 1991. Antarctic mesocyclone regimes from satellite and conventional data. *Tellus* **44A**, 180–196.

Franzke, C., Majda, A. J. and Vanden-Eijnden, E. 2005. Low-order stochastic mode reduction for a realistic barotropic model climate. *J. Atmos. Sci.* **62**, 1722–1745.

Goswami, B. N., Ajayamohan, R. S., Xavier, P. K. and Sengupta, D. 2003. Clustering of synoptic activity by Indian summer monsoon intraseasonal oscillations. *Geophys. Res. Lett.* **30**, 1431.

Green, J. 1970. Transfer properties of the large-scale eddies and the general circulation of the atmosphere. *Quart. J. R. Met. Soc.* **96**, 157–185.

Gryanik, V. and Hartmann, J. 2002. A turbulence closure for the convective boundary layer based on a two-scale mass-flux approach. *J. Atmos. Sci.* **59**, 2729–2744.

Gryanik, V. M., Hartmann, J., Raasch, S. and Schroeter, M. 2005. A refinement of the Millionshchikov quasi-normality hypothesis for convective boundary layer turbulence. *J. Atmos. Sci.* **62**, 2632–2638.

Gyakim, J. R. and Barker, E. S. 1988. A case study of explosive subsynoptic-scale cyclogenesis. *Mon. Wea. Rev.* **116**, 2225–2253.

Hakim, G. J. and Canavan, A. K. 2005. Observed cyclone-anticyclone tropopause vortex asymmetries. *J. Atmos. Sci.* **62**, 231–240

Hakim, G. J., Snyder, C. and Muraki, D. J. 2002. A new surface model for cyclone-anticyclone asymmetry. *J. Atmos. Sci.* **59**, 2405–2420.

Handorf, D., Petoukhov, V. K., Dethloff, K., Eliseev, A. V., Weisheimer, A. and Mokhov, I. I. 1999. Decadal climate variability in a coupled atmosphere-ocean climate model of moderate complexity. *J. Geophys. Res.* **104**, 27 253–27 275.

Heinemann, G. 1990. Mesoscale vortices in the Weddel Sea region (Antarctica). *Mon. Wea. Rev.* **118**, 779–793.

Heinemann, G. and Klein, T. 2003. Simulations of topographically forced mesocyclones in the Weddel Sea and the Ross Sea region of Antarctica. *Mon. Wea. Rev.* **131**, 302–316.

Holzer, M. 1996. Asymmetric geopotential height fluctuations from symmetric winds. *J. Atmos. Sci.* **53**, 1361–1379.

Hoskins, B. 1996. On the existence and strength of the summer subtropical anticyclones—Bernhard Haurwitz memorial lecture. *Bull. Am. Meteorol. Soc.* **77**, 1287–1292.

Hoskins, B. J. and Hodges, K. I. 2002. New perspectives on the Northern Hemisphere winter storm tracks. *J. Atmos. Sci.* **59**, 1041–1061.

Hoskins, B. J. and Hodges, K. I. 2005. New perspectives on the Southern Hemisphere winter storm tracks. *J. Climate* **18**, 4108–4129.

Hsu, H.-H. 2005. East Asian monsoon. In: *Intraseasonal Variability in the Atmosphere-Ocean Climate System* (eds W. K.-M. Lau and D. Waliser), Springer-Verlag, Berlin, 63–90.

Hu, Y. and Pierrehumbert, R. T. 2001. The advection-diffusion problem for stratospheric flow. Part I: concentration probability distribution function. *J. Atmos. Sci.* **58**, 1493–1510.

James, I. N. 2001. Some aspects of the global circulation in January and July 1980. In: *Large-Scale Dynamical Processes in the Atmosphere*. (eds B. Hoskins and R. Pearse), Academic Press, New York, 5–26.

James, R. W. 1952. On the vertical structure of pressure and wind-fields. *Meteorol. Atmos. Phys.* **5**, 17–35.

Jones, C. and Carvalho, L. M. V. 2002. Active and break phases in the South American monsoon system. *J. Climate* **15**, 905–914.

Kiladis, G. N. and Weickmann, K. M. 1992. Extratropical forcing of tropical Pacific convection during northern winter. *Mon. Wea. Rev.* **120**, 1924–1938

Knox, R. 1987. The Indian Ocean: interaction with the monsoon. In: *Monsoons*. (eds J. S. Fein and P. L. Stephens), John Wiley, New York, 365–398.

Kraichnan, R. H. 1959. The structure of isotropic turbulence at very high Reynolds numbers. *J. Fluid Mech.* **5**, 497–543.

Kuo, A. C. and Polvani, L. M. 2000. Nonlinear geostrophic adjustment, cyclone/anticyclone asymmetry, and potential vorticity rearrangement. *Phys. Fluids* **12**, 1087–1100.

Kurihara, Y. 1970. A statistical-dynamical model of the general circulation of the atmosphere. *J. Atmos. Sci.* **27**, 847–870.

Lamb, H. 1975 *Hydrodynamics*, Cambrige Univ. Press, London.

Lapeyre, G. and Held, I. M. 2004. The role of moisture in the dynamics and energetics of turbulent baroclinic eddies. *J. Atmos. Sci.* **61**, 1693–1710.

Larichev, V. D. and Held, I. M. 1995. Eddy amplitudes and fluxes in a homogeneous model of fully developed baroclinic instability. *J. Phys. Oceanogr.* **25**, 2285–2297.

Lau, N.–C. 1979. The structure and energetics of the transient disturbances in the Northern Hemisphere wintertime circulation. *J. Atmos. Sci.* **36**, 982–995.

Lau, N.-C. 1988. Variability of the observed midlatitude storm tracks in relation to low-frequency changes in the circulation pattern. *J. Atmos. Sci.* **45**, 2718–2743.

Lau, N.-C. and Wallace, J. 1979. On the distribution of horizontal transports by transient eddies in the northern hemisphere wintertime circulation. *J. Atmos. Sci.* **36**, 1844–1861.

Lorenz, E.N. 1967. *The Nature and Theory of the General Circulation of the Atmosphere*, World Meteorological Organization, Geneva.

Lorenz, E. 1979. Forced and free variations of weather and climate. *J. Atmos. Sci.* **36**, 1367–1376.

Lorenz, D. J. and Hartmann, D. L. 2001. Eddy-zonal flow feedback in the Southern Hemisphere. *J. Atmos. Sci.* **58**, 3312–3327.

Majda, A. J., Timofeyev, I. and Vanden-Eijnden, E. 2001. A mathematical framework for stochastic climate models. *Comm. Pure Appl. Math.* **54**, 891–974.

Mak, M. 1987. Synoptic-scale disturbances in the summer monsoon. In: *Monsoon Meteorology*. (eds C. P. Chang and T. N. Krishnamurti), Oxford University Press, New York, 435–460.

McComb, W. D. 1992. *The Physics of Fluid Turbulence.* Oxford University Press, Oxford.

Methven, J. and Hoskins, B. 1998. Spirals in potential vorticity. Part I: measures of structure. *J. Atmos. Sci.* **55**, 2053–2066.

Monahan, A. H. 2004. Low-frequency variability of the statistical moments of sea surface winds. *Geophys. Res. Lett.* **31**, L10302.

Monahan, A. H. 2006a. The probability distribution of sea surface wind speeds. Part I: theory and SeaWinds observations. *J. Climate* **19**, 497–520.

Monahan, A. H. 2006b. The probability distribution of sea surface wind speeds. Part II: dataset intercomparison and seasonal variability. *J. Climate* **19**, 521–534.

Monin, A. 1958. On tentative computation of atmospheric zonal circulation characteristics. *Izvestiya, Geophysics (Izvestiya Akademii Nauk SSSR, Seriya Geofizicheskaya)* **10**, 1250–1253.

Monin, A. and Yaglom, A. M. 1981. *Statistical Fluid Mechanics: Mechanics of Turbulence*, MIT Press, Cambridge, MA.

Morris, W. E. and Smith, P. J. 2001. Cyclolysis: a diagnosis of two extratropical cyclones. *Mon. Wea. Rev.* **129**, 2714–2729.

Murakami, M. 1979. Large-scale aspects of deep convective activity over the GATE area. *Mon. Wea. Rev.* **107**, 994–1013.

Nakamura, H. and Shimpo, A. 2004. Seasonal variations in the Southern Hemisphere storm tracks and jet streams as revealed in a reanalysis dataset. *J. Climate* **17**, 1828–1844.

Ogura, Y. 1962. Energy transfer in a normally distributed and isotropic turbulent velocity field in two dimensions. *Phys. Fluids* **5**, 395–401.

Oort, A. 1983. Global atmospheric circulation statistics, 1958–1973, *Tech. Rep. NOAA Prof. Pap. No. 14*, Govt. Printing Office, Washington, DC.

Opsteegh, J. and van den Dool, H. 1979. A diagnostic study of the time -mean atmosphere over the northwestern Europe during winter. *J. Atmos. Sci.* **36**, 1862–1879.

Orlanski, I. and Gross, B. 2000. The life cycle of baroclinic eddies in a storm track environment. *J. Atmos. Sci.* **57**, 3498–3513.

Palmen, E. and Newton, C. W. 1969. *Atmospheric circulation systems*. (ed. W. L. Donn), Academic Press, New York.

Palmer, T. N. 1994. Chaos and the predictability in forecasting the monsoons. *Proc. Indian. Nat. Sci. Acad., Part A* **60**, 57–66.

Pavan, V. and Held, I. 1996. The diffusive approximation for eddy fluxes in baroclinically unstable jets. *J. Atmos. Sci.* **53**, 1262–1272.

Peixoto, J. P. and Oort, A. H. 1992. *Physics of Climate*, American Institute of Physics, New York.

Petoukhov, V. 1980. Zonal climatic model of heat and moisture exchange in the atmosphere over underlying layer. In: *Studies of Eddy Dynamics, Atmospheric Energetics and the Problem of Climate*, (eds E. Nikiforov and V. Ph. Romanov), Gidrometeoizdat, Leningrad. 8–41.

Petoukhov, V. K., Mokhov, I. I., Eliseev, A. V. and Semenov, V. A. 1998. *The IAP RAS Global Climate Model*, Dialogue-MSU, Moscow.

Petoukhov, V., Ganopolski, A., Brovkin, V., Claussen, M., Eliseev, A., and co-authors. 2000. CLIMBER-2: a climate system model of intermediate complexity. Part I: model description and performance for present climate. *Clim. Dyn.* **16**, 1–17.

Petoukhov, V., Ganopolski, A. and Claussen, M. 2003. POTSDAM—a set of atmosphere statistical-dynamical models: theoretical background, *Tech. Rep. PIK Rep. 81*, Potsdam-Institut für Klimafolgenforschung, Potsdam.

Petoukhov, V., Claussen, M., Berger, A., Crucifix, M., Eby, M., and co-authors. 2005. EMIC intercomparison project (EMIP-CO2): comparative analysis of EMIC simulations of current climate and equilibrium and transient responses to atmospheric CO_2 doubling. *Clim. Dyn.* **25**, 363–385.

Petterssen, S. 1950. Some aspects of the general circulation of the atmosphere. *Cent. Proc. Roy. Meteor. Soc.*, **17**, 120–155.

Pierrehumbert, R. T. 1991. Chaotic mixing of tracer and vorticity by modulated traveling Rossby waves. *Geophys. Astrophys. Fluid Dyn.* **58**, 285–320.

Ramage, C. S. 1971. *Monsoon Meteorology.* Academic Press, New York.

Randel, W. and Held, I. 1991. Phase speed spectra of transient eddy fluxes and critical layer absorption. *J. Atmos. Sci.* **48**, 688–697.

Randall, D. A., Shao, Q. and Moeng, C.-H. 1992. A second-order bulk boundary-layer model. *J. Atmos. Sci.* **49**, 1903–1923.

Rhines, P. B. 1975. Waves and turbulence on a beta-plane. *J. Fluid Mech.* **69**, 417–443.

Riehl, H. 1979. *Climate and weather in the tropics.* Academic Press, New York.

Rivin, I. and Tziperman, E. 1997. Linear versus self-sustained interdecadeal thermochaline variability in a coupled box model. *J. Phys. Oceanogr.* **27**, 1216–1232.

Rodwell, M. J. and Hoskins, B. J. 2001. Subtropical anticyclones and summer monsoons. *J. Climate* **14**, 3192–3211.

Salmon, R. 1998. *Lectures on Geophysical Fluid Dynamics*, Oxford University Press, Oxford.

Saltzman, B. 1978. A survey of statistical-dynamical models of the terrestrial climate. *Adv. Geophys.* **20**, 183–304.

Saltzman, B. and Vernekar, A. 1971. An equilibrium solution for the axially symmetric component of the Earth's macroclimate. *J. geophys. Res.* **76**, 1498–1524.

Saltzman, B., Guttoso, R. and Fleisher, A. 1961. The meridional eddy transport of kinetic energy at 500 mbar. *Tellus*, **13**, 293–295.

Schmittner, A., Appenzeller, C. and Stocker, T. 2000. Validation of parameterisations for the meridional energy and moisture transport used in simple climate models. *Clim. Dyn.* **16**, 63–77.

Schumann, U. 1977. Realizability of Reynolds-stress turbulence models. *Phys. Fluids.* **20**, 721–725.

Simmonds, I. 2000. Size changes over the life of sea level cyclones in the NCEP reanalysis. *Mon. Wea. Rev.* **128**, 4118–4125

Simmonds, I. and Keay, K. 2000. Mean Southern Hemisphere extratropical cyclone behavior in the 40-year NCEP-NCAR reanalysis. *J. Climate* **13**, 873–885

Simmons, A. and Gibson, J. 2000. The ERA-40 project plan. *ERA-40 Project Rep. Ser. 1*, European Center for Medium–Range Weather Forecasting, Reading.

Simmons, A. J. and Hoskins, B. J. 1978. The life cycles of some nonlinear baroclinic waves. *J. Atmos. Sci.* **35**, 414–432.

Simmons, A. J. and Hoskins, B. J. 1980. Barotropic influences on the growth and decay of nonlinear baroclinic waves. *J. Atmos. Sci.* **37**, 1679–1684.

Sinclair, M. R. 1997. Obvjective identification of cyclones and their circulation intensity, and climatology. *J. Atmos. Sci.* **12**, 595–612.

Sinclair, M. R. and Watterson, I. G. 1999. Objective assessment of extratropical weather systems in simulated climates. *J. Climate*, **12**, 3467–3485.

Srivatsangam, S. 1978. Parametric study of large-scale eddy properties. part I: eddy fluxes. *J. Atmos. Sci.* **35**, 1212–1219.

Stone, P. 1978. Baroclinic adjustment. *J. Atmos. Sci.* **35**, 561–571.

Sura, P., Newman, M., Penland, C., and Sardeshmukh, P. 2005. Multiplicative noise and non–gaussianity: a paradigm for atmospheric regimes?. *J. Atmos. Sci.* **62**, 1391–1409.

Swanson, K. and Pierrehumbert, R. 1997. Lower-tropospheric heat transport in the Pacific storm track. *J. Atmos. Sci.* **54**, 1533–1543.

Tomas, R. and Webster, P. J. 1997. On the location of the intertropical convergence zone and near-equatorial convection: The role of internal instability. *Quart. J. R. Met. Soc.* **123**, 1445–1482.

Trenberth, K. 1991. Storm tracks in the Southern Hemisphere. *J. Atmos. Sci.* **48**, 2159–2178.

Trigo, I. F. 2006. Climatology and interannual variability of storm-tracks in the Euro-Atlantic sector: a comparison between ERA-40 and NCEP/NCAR reanalyses. *Clim. Dyn.* **26**, 127–143.

Wallace, J., Lim, G. and Blackmon, M. 1988. Relationship between cyclone tracks, anticyclone tracks, and baroclinic waveguides. *J. Atmos. Sci.* **45**, 439–462.

Weaver, C. and Ramanathan, V. 1997. Relationships between large-scale vertical velocity, static stability, and cloud radiative forcing over the Northern Hemisphere extratropical latitudes. *J. Climate* **10**, 2871–2887.

Webster, P. J., Magana, V. O., Palmer, T. N., Shukla, J., Tomas, R. A., and co-authors. 1998. Monsoons: processes, predictability, and the prospects for prediction. *J. geophys. Res.* **103**, 14451–14510.

Welch, W. and Tung, K.-K. 1998a. Nonlinear baroclinic adjustment and wave number selection in a simple case. *J. Atmos. Sci.* **55**, 1285–1302.

Welch, W. and Tung, K.-K. 1998b. On the equilibrium spectrum of transient waves in the atmosphere. *J. Atmos. Sci.* **55**, 2833–2851.

Whitaker, J. S. and Sardeshmukh, P. D. 1998. A linear theory of extratropical synoptic eddy statistics. *J. Atmos. Sci.* **55**, 237–258.

White, G. 1980. Skewness, kurtosis and extreme values of northern hemisphere geopotential heights. *Mon. Wea. Rev.* **108**, 1446–1455.

Wiin-Nielsen, A. 1974. Vorticity, divergence and vertical velocity in a baroclinic boundary layer with a linear variation of the geostrophic wind. *Boundary-Layer Meteorol.* **6**, 459–476.

Williams, G. and Davies, D. 1965. A mean motion model of the general circulation. *Quart. J. R. Met. Soc.* **91**, 471–489.

Zhang, Y. and Held, I. 1999. A linear stochastic model of a GCM's midlatitude storm tracks. *J. Atmos. Sci.* **56**, 3416–3435.